LOW-ENERGY PROTONS FROM TARGETS BOMBARDED BY 15-MEV DEUTERONS

by

Frank A. Aschenbrenner

B.S., Kansas State College

(1950)

SUBMITTED IN PARTIAL FULFILLMENT OF THE

REQUIREMENTS FOR THE DEGREE OF

DOCTOR OF PHILOSOPHY

at the

MASSACHUSETTS INSTITUTE OF TECHNOLOGY

1954

Signature of Author_____
Department of Physics, May 1954

Certified by_____
Thesis Supervisor

_____
Chairman, Departmental Committee on Graduate Students

LOW-ENERGY PROTONS FROM TARGETS BOMBARDED BY 15-MEV DEUTERONS

Frank A. Aschenbrenner

Submitted to the Department of Physics
on May 17, 1954 in partial fulfillment
of the requirements for the degree of
Doctor of Philosophy

ABSTRACT

A particle-selection technique is described which makes it possible to identify readily the reaction particles from deuteron-induced reactions. The results of a study of the low-energy protons from targets bombarded by 15-Mev deuterons is presented.

The deuteron beam from the M.I.T. Cyclotron was used to bombard thin targets in the center of a scattering chamber. The reaction particles were detected with a counter combination which consists of two scintillation counters mounted on one movable arm in the scattering chamber. The first is a thin plastic scintillation counter which measures dE/dx of the reaction particles, and the second is a NaI(Tl) scintillation counter which measures the remaining energy of the reaction particles after they pass through the thin counter. With appropriate electronic apparatus, the information from the two counters was used to obtain the energy spectra of the emitted protons.

The proton energy spectra from niobium, silver, antimony, tantalum, three lead isotopes, and uranium bombarded with the direct deuteron beam were observed at several angles. In addition, the proton energy spectrum from tantalum was observed at several deuteron beam energies ranging from approximately 10.5 to 15 Mev. In these measurements, the direct deuteron beam energy was reduced by inserting aluminum foils.

The low-energy parts of the proton spectra show what appears to be a coulomb barrier effect. However, protons are observed several

Mev below the coulomb barrier for protons, indicating that the barrier effect differs from the ordinary coulomb barrier penetration of protons emerging from a compound nucleus. The behavior of the barrier effect with respect to changes in counter angle, Z (atomic number) and A (mass number) of the targets and deuteron beam energy was noted.

All the properties of the low-energy parts of the proton spectra appear to be consistent with a stripping model in which the deuteron is first polarized and stretched by the coulomb field and then the neutron is stripped off by the nucleus leaving the proton outside the coulomb barrier. This interpretation is supported by a comparison of the angular distribution and estimated cross sections for the protons with $Q < -2.23$ Mev with the angular distributions and estimated cross sections for the protons with $Q > -2.23$ Mev.

It is suggested that a variation of an existing semiclassical formulation, which was used for calculating (d,p) excitation functions, can be used to explain the low-energy parts of the proton spectra.

Thesis Supervisor: M. Stanley Livingston

Title: Professor of Physics

A C K N O W L E D G M E N T S

The author would like to thank Professor M. S. Livingston, under whose direction this work was carried out. His advice and suggestions were very helpful.

The author is grateful to Dr. K. Boyer of Los Alamos for suggesting the importance of studying the low-energy protons. He is also grateful to Professor V. Weisskopf and Professor F. Friedman for valuable discussions on the theoretical implications of the results.

Sincerest appreciation is extended to Mr. H. S. Stoddart for his design of a large part of the electronic apparatus and for the many suggestions which were extremely helpful in developing the particle selection technique.

Appreciation is also extended to Dr. N. S. Wall and Mr. J. W. Haffner for their general assistance and helpful suggestions.

The author is indebted to Mr. F. Fay, Mr. A. Nummela, and Mr. E. White of the M.I.T. Cyclotron crew for their efficient help in the building and maintenance of the experimental apparatus.

TABLE OF CONTENTS

LIST OF FIGURES

LIST OF TABLES

I. INTRODUCTION

When thin targets are bombarded with deuterons, several types of particles are emitted. Of these, protons and neutrons have been found to be the most abundant. In general, the yield for deuteron-induced reactions is much larger than that of corresponding reactions with other charged particles. For this reason, deuterons are commonly accelerated in cyclotrons for the purpose of radioactive isotope production.

In recent years (d,p) reactions have been subjected to large numbers of experimental and theoretical investigations. In general these investigations have been conducted for two purposes. These are:

1. A study of the properties of the energy levels of the residual nuclei through observations of the proton energy groups;

2. A study of the mechanism of the (d,p) reaction.

Symbolically, the (d,p) reaction can be written $X + d \longrightarrow Y + p + Q$, where X is the target nucleus; Y is the residual nucleus; and Q is the reaction energy balance, commonly called the Q of the reaction. For Q greater than -2.23 Mev (where 2.23 Mev is the binding energy of the deuteron), the residual nucleus is stable against neutron emission and, in general, against any heavy particle emission. For Q less than or equal to -2.23 Mev, sufficient energy has been transferred to the residual nucleus to allow neutron emission. In this case the reaction can be written:

$$X + d \longrightarrow Y + p + Q \longrightarrow (X + n) + p + Q.$$

It is obvious that for Q = -2.23 Mev sufficient energy has been supplied by the kinetic energy of the deuteron to separate the proton and neutron in the deuteron.

For the cases when neutron emission is possible ($Q < -2.23$ Mev) the energy-level widths are much larger than for the cases when neutron emission is not possible. Except for very light nuclei, the level widths when neutron emission is possible are greater than the level separations. Therefore, observation of the proton spectra for $Q < -2.23$ Mev in heavy nuclei gives information on level densities rather than on discrete energy levels. This region is generally referred to as a continuum.

The (d,p) reactions with $Q > -2.23$ Mev (assuming that 2.23 Mev is the binding energy of the deuteron) can occur in two possible ways. The first possibility is for the deuteron to enter the nucleus as a unit, forming a compound nucleus with the subsequent emission of a proton. The very high cross sections observed with low deuteron bombarding energies could not be explained by this picture, in which the deuterons were required to penetrate the coulomb barrier. In order to explain these high cross sections, Oppenheimer and Phillips (O1) proposed that the deuteron is polarized in the coulomb field of the nucleus and the neutron is captured without the proton entering the nucleus. Later, Peaslee (P1) concluded that the compound-nucleus formation is less important than the Oppenheimer-Phillips, or stripping, reaction at all deuteron bombarding energies. Peasles success-

fully formulated a semiclassical theory that is in agreement with observed (d,p) excitation functions.

More recently, a wave-mechanical description of the (d,p) stripping reaction was formulated by Butler (B1) which neglected coulomb effects. The agreement between experimental data (B2) and Butler's formulation, in which the neutron is captured by the target nucleus, indicates that the (d,p) reactions are almost entirely due to stripping. This agreement has made it possible to determine the orbital quantum number of the captured neutron.

The protons with energies corresponding to (d,p) reactions with $Q < -2.23$ Mev can result from another process. This is the electric breakup of the deuteron by the coulomb field of the nucleus. Cross sections for the electric breakup process have been calculated by Guth and Mullin (G3) to be of the order of 200 millibarns for targets of $Z > 29$ bombarded with 15-Mev deuterons. This would predict a strong competition between the electric breakup process and (d,p) stripping.

Because of experimental difficulties, the protons with energies corresponding to (d,p) reactions with $Q < -2.23$ Mev had not in the past been observed, However, the recent development of a convenient particle-selection technique at the M. I. T. Cyclotron has made it possible to study the entire proton spectra from targets with $Z > 41$. It was decided to conduct a study of the low-energy protons from selected targets bombarded with the M. I. T. Cyclotron

deuteron beam which would determine what processes are most important in producing the low-energy protons. The results indicate that the low-energy protons are also almost entirely due to (d,p) stripping. It is believed that a slight variation of Peaslee's semiclassical formulation can be used to explain the low-energy proton spectra.

II. APPARATUS

A. CYCLOTRON AND EMERGENT BEAM

The source of high-energy deuterons used for these experiments has been the M. I. T. Cyclotron, which produces an external beam of approximately 15 Mev (L1). The cyclotron is housed in a vault with 4-foot thick concrete walls that serve to protect the personnel and reduce the background radiation at the scattering chamber. The scattering chamber is located in an adjacent vault which has 2-foot thick concrete walls. The scattering chamber is connected to the cyclotron with a tube through which the deuterons are conducted. The tube contains several tantalum baffles to prevent the target from seeing small-angle scattered deuterons. A defining aperture is placed at the entrance of the scattering chamber. The deuterons are focused on the target at the center of the scattering chamber with a focus magnet that is located in the cyclotron vault. The focus magnet can be remotely controlled from the outside area. The optimum setting of the focus magnet is obtained by requiring a maximum reading in the Faraday cup in the beam catcher beyond the scattering chamber. This focusing system produces a spot on the target that is approximately 1/4-inch wide and 3/8-inch high. Figure 1 shows a schematic diagram of the cyclotron and emergent beam equipment.

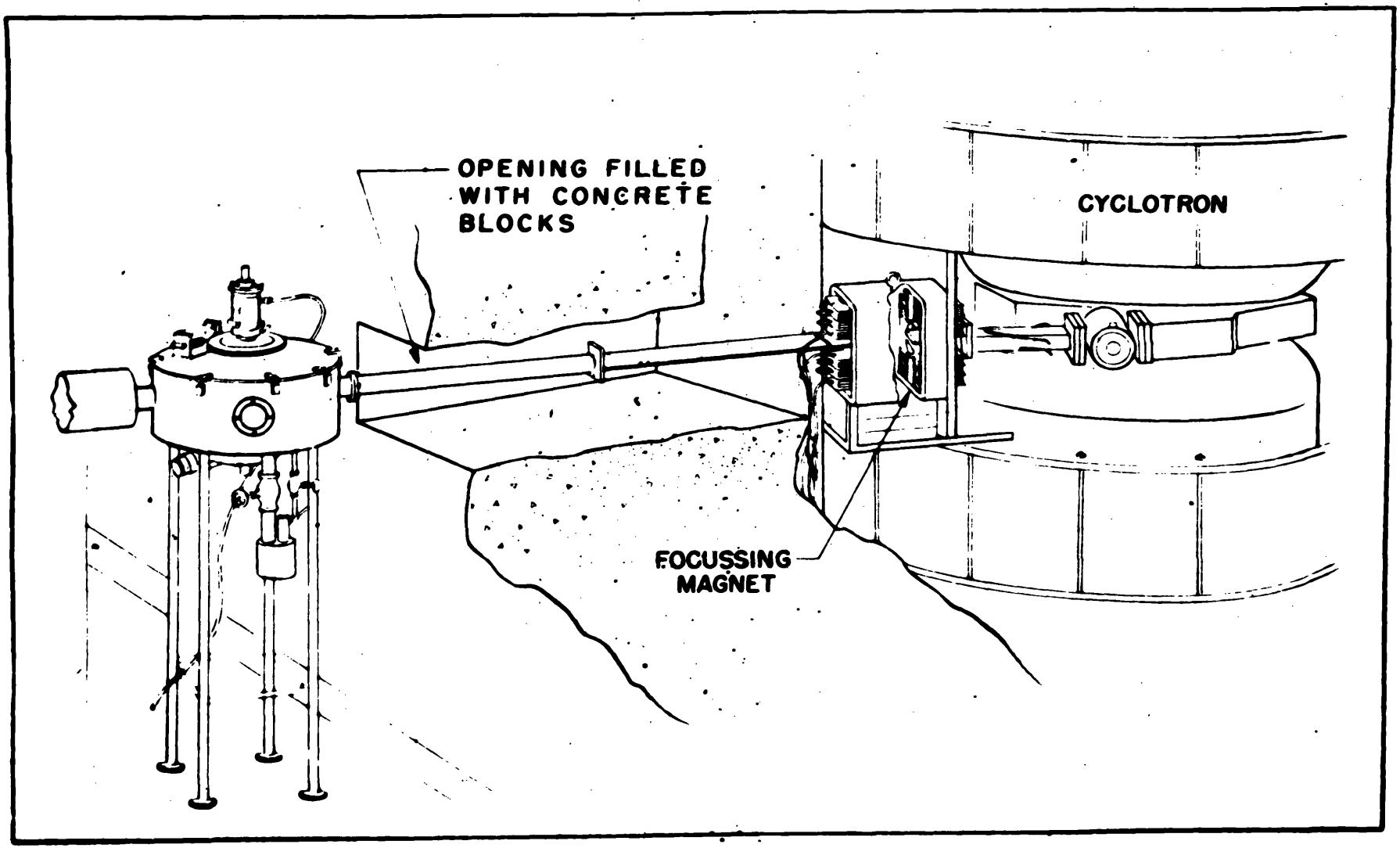
OPENING FILLED
WITH CONCRETE
BLOCKS
CYCLOTRON
FOCUSSING
MAGNET

For some of the experiments, a foil changer was placed between the conducting tube and the scattering chamber. This foil changer made it possible to insert aluminum foils in the deuteron beam to reduce the beam energy at the target.

The scattering chamber has been previously described by Harvey (H1).

B. BEAM MONITOR

Except for minor changes, the deuteron beam monitor used in these experiments is the same as described by Wall (W1). Briefly, the monitor counter consists of a scintillation counter which is placed in a port at an angle of 45 degrees from the deuteron beam between the scattering chamber and the beam catcher. A thin gold foil is inserted in the beam at this point so that particles scattered 45 degrees by the foil are observed by the monitor counter. The scintillation counter consists of a 6291 Dumont photomultiplier tube and a plastic scintillator.* The optics of this counter is similar to that described by Stoddart and Gove (S1). The resolution of this counter for 15-Mev dueterons scattered elastically from the gold foil is 5 percent.

C. PARTICLE SELECTIVE COUNTER

The particle selective counter consists of two scintillation counters (Figures 2 and 3). The first is a thin plastic scintilla-

*The plastic scintillator was obtained from Pilot Chemicals, Inc., 47 Felton Street, Waltham, Massachusetts.

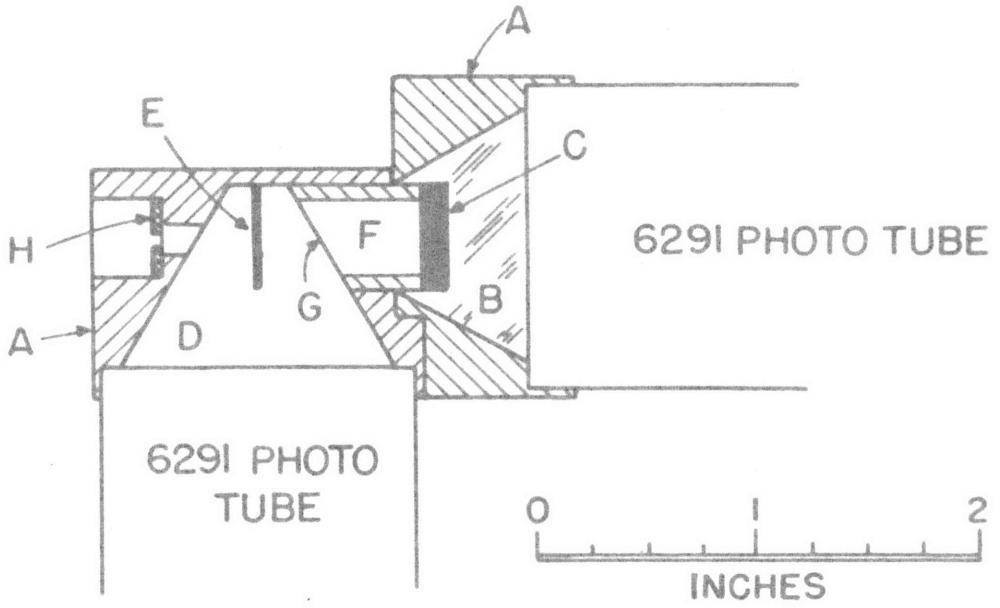

A. ALUMINUM

B. LUCITE

C. NaI (Tl)

D. SPACE

E. PLASTIC SCINTILLATOR

F. ALUMINUM CYLINDER

G. ALUMINUM FOIL

H. LEAD

Figure 2

PARTICLE SELECTIVE COUNTER

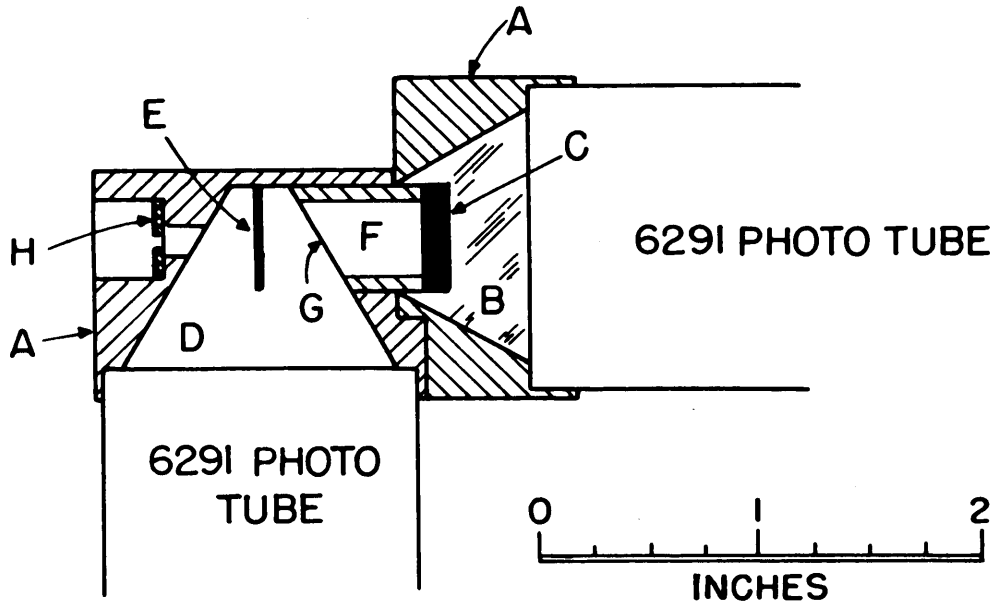

A. ALUMINUM

B. LUCITE

C. NaI (Tl)

D. SPACE

E. PLASTIC SCINTILLATOR

F. ALUMINUM CYLINDER

G. ALUMINUM FOIL

H. LEAD

PARTICLE SELECTIVE COUNTER

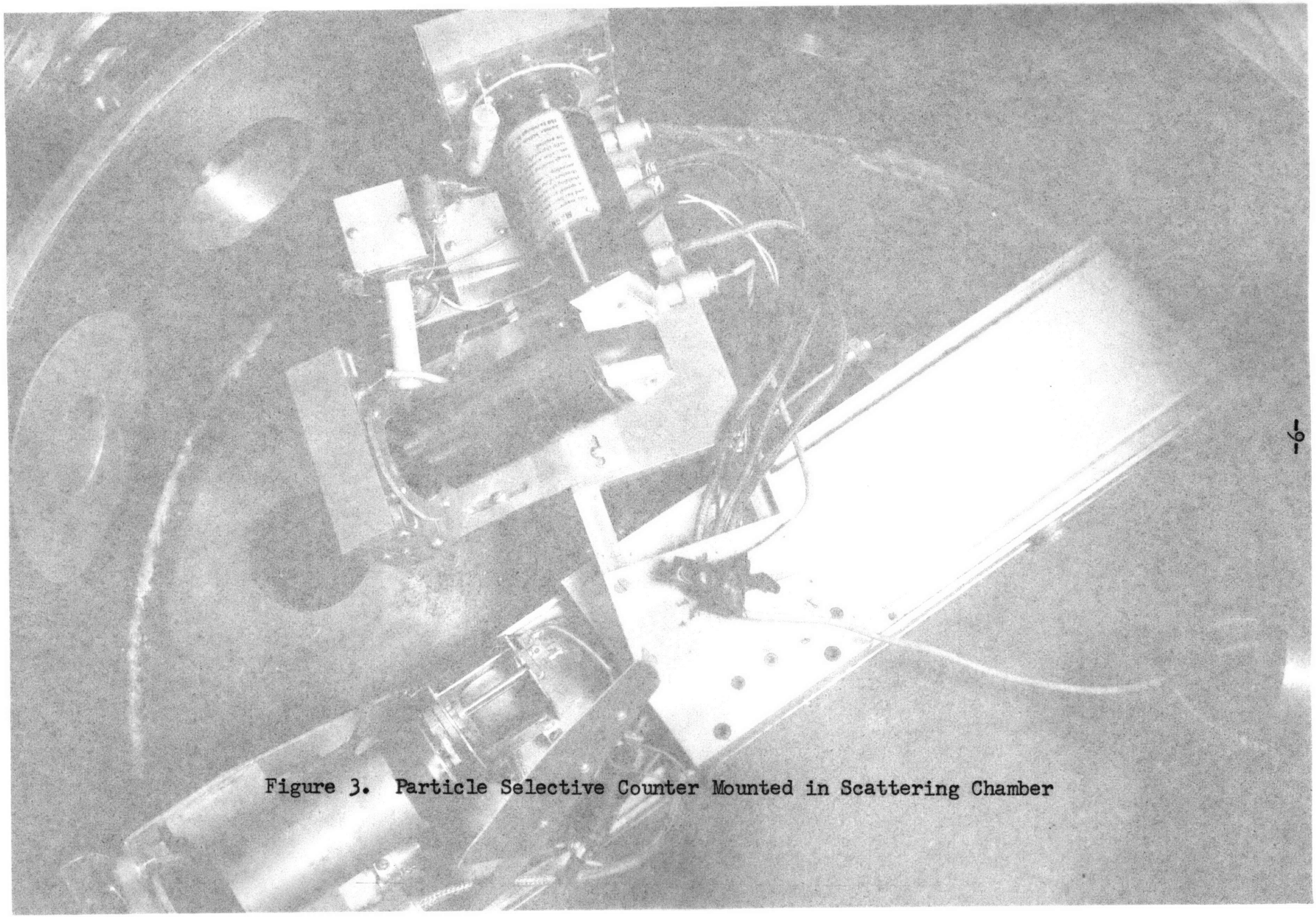

Figure 3. Particle Selective Counter Mounted in Scattering Chamber

MAGNETIC

tion counter which measures the initial specific ionization of the reaction particles. The second is a NaI(Tl) scintillation spectrometer which measures the remaining energy of the reaction particles after they pass through the thin counter. The combined information from these counters makes it possible to identify protons, deuterons, tritons, and alpha-particles with ranges large enough to pass through the first counter and strike the NaI(Tl) crystal.

Calculations from range-energy curves show that protons, deuterons, and tritons with equal incident energies lose amounts of energy in the plastic scintillator in the ratios 1:1.8:2.6. However, since plastic scintillators have a nonlinear response for particles of high dE/dx similar to stilbene and anthracene (Tl), the ratios of the pulses for these particles coming from the thin counter deviate from the calculated ratios. The deviations depend upon the incident energies. Because the information from the thin counter is used only to identify the reaction particles, these deviations are serious only at a part of the energy spectrum. The limitations of this counter combination, which are due to the nonlinear response of the plastic scintillator, will be discussed further in the section entitled "Particle Selection Technique."

During most of the experiments, a 28 mgs/cm^2 thick Pilot Scintillator B was used in the first counter. The scintillator was machined to this thickness from a larger piece with the cyclotron

machine-shop lathe. The resolution obtained for 15-Mev deuterons scattered 45 degrees elastically with a thin gold foil was 13 percent. In this case, the deuterons lost approximately 2 Mev in the plastic scintillator.

D. ELECTRONIC APPARATUS

Some of the electronic apparatus has been previously described by Wall (W1); therefore, only the modifications of this apparatus will be discussed here. To facilitate particle selection, it was necessary to add several pieces of electronic apparatus having special purposes. This apparatus will be described in this section. The reasons for requiring the additional apparatus will be discussed in the section entitled "Particle Selection Technique." Figure 12 shows a block diagram of the electronic apparatus used.

1. Pulse Shaper. Since pulses coming from NaI(Tl) scintillation counters have relatively long rise times, it is necessary to shape the pulses so that they have flat tops approximately 3 microseconds long for the oscilloscope display system. A single-stage delay-line pulse shaper would not return the pulses to zero after shaping because of the amplitude attenuation of the reflected pulses in the long delay line. However, a double-stage delay-line pulse shaper with two identical stages will return the pulses much closer to zero after two pulse lengths. Figure 4 shows a schematic diagram of the pulse shaper used and sketches of the pulses obtained

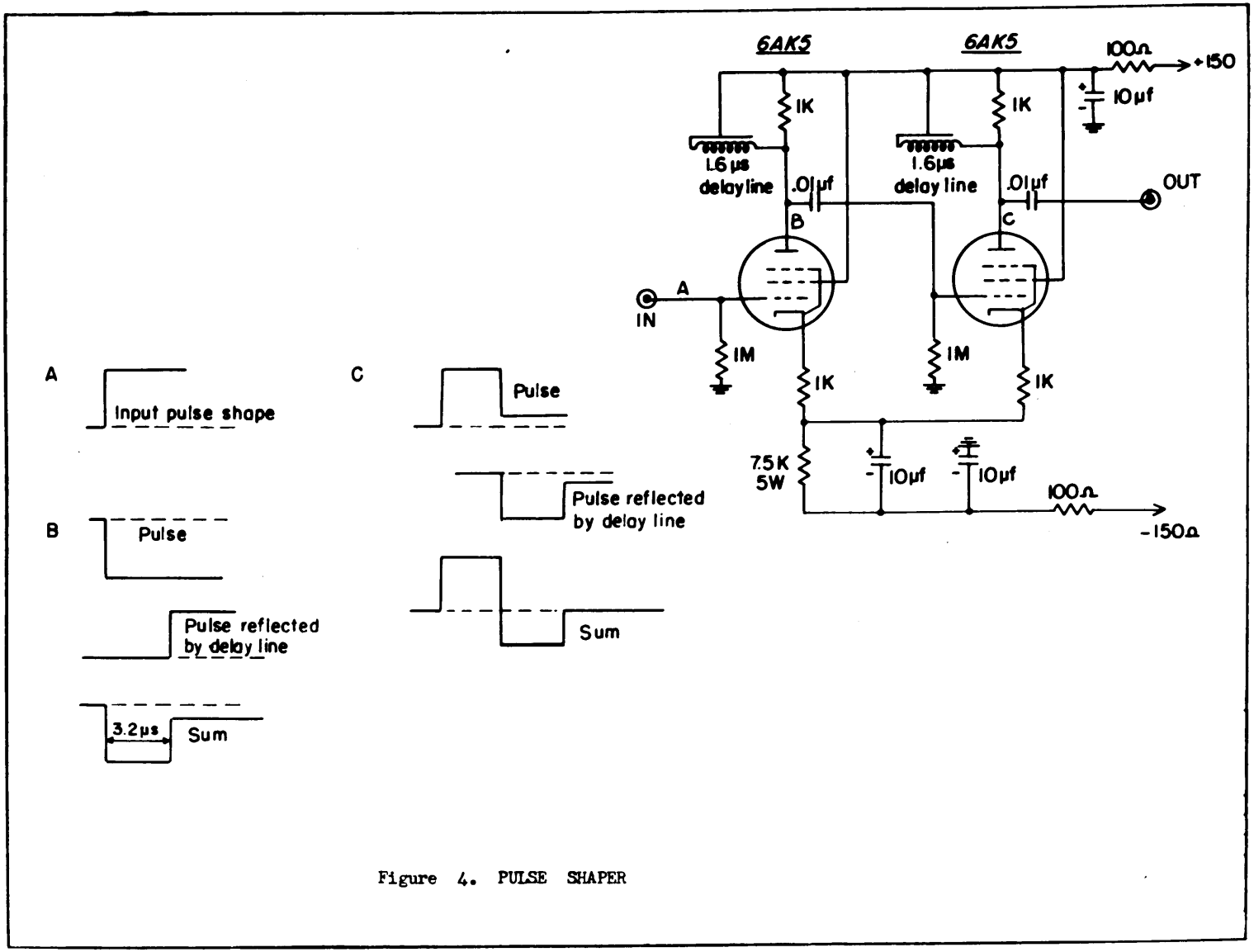

Figure 4. PULSE SHAPER

after each stage under ideal conditions. Figures 5(a) and 5(b) show pictures taken with a Polaroid Land Camera of actual pulses displayed on an oscilloscope. It was not necessary to get rid of the negative parts of the pulses because the pulse multiplier and the pulse height analyzers are insensitive to negative pulses.

2. Pulse Adder. The pulses from the two scintillation counters are fed into the grids of a double triode (see Figure 7). The adding is done by superposing the plate currents through a common resistor. Since the gains of the amplifiers used with the counters are not necessarily the same, a control is provided that changes the gain of one side of the double triode relative to the other side. This makes it possible to obtain an output which is proportional to $E_1 + E_2$ where E_1 is the energy the particles lose in the thin counter, and E_2 is the energy the particles lose in the NaI(Tl) counter.

Included with the adder circuit are two cathode follower outputs. One output is the sum $E_1 + E_2$, and the other is E_1. The two outputs are connected to the inputs of the pulse multiplier. Cathode follower outputs are required because the pulses are fed into the grids of twenty-five 6BN6 tubes in the pulse multiplier. The gains are adjusted at this point so that the range of pulse heights from each output is between 0 and 12 volts, which is the range required by the pulse multiplier.

3. Pulse Multiplier. The pulse multiplying is done with a 5 x 5 array of 6BN6 tubes. The characteristics of a 6BN6 tube

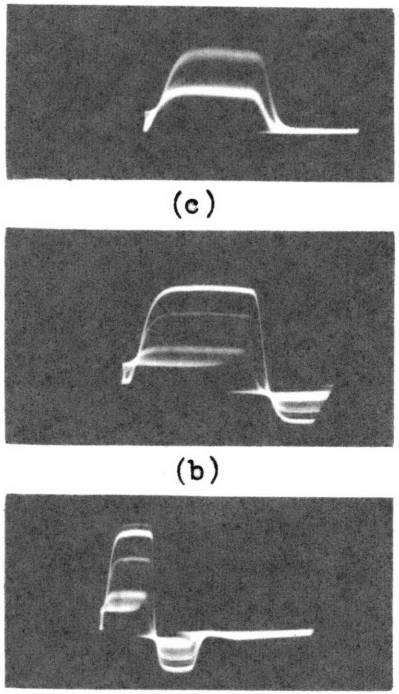

Figure 5
Photograph of oscilloscope screen showing pulse shapes. (a), (b). Pulses from counters after pulse shaping. Sweep speed faster in (b). (c) Pulses from multiplier.

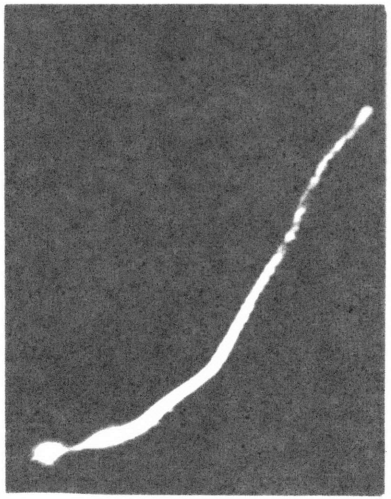

Figure 6
Photograph of oscilloscope screen showing performance of pulse multiplier when the same pulses are fed into both inputs. Input on X-axis. Output on Y-axis.

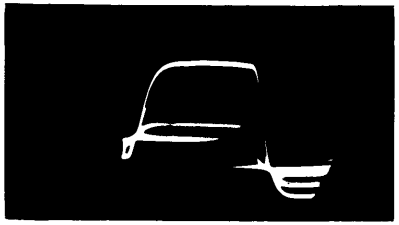

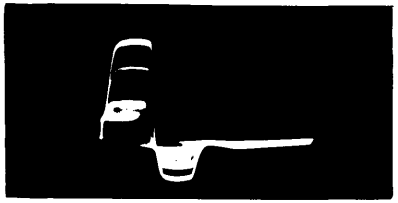

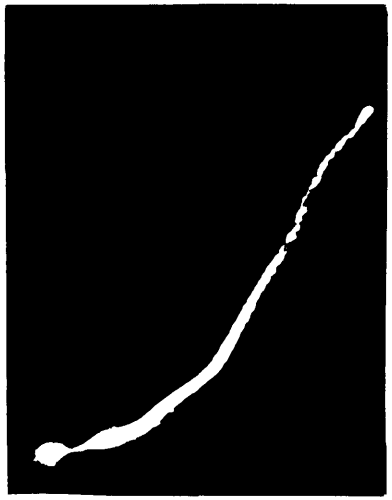

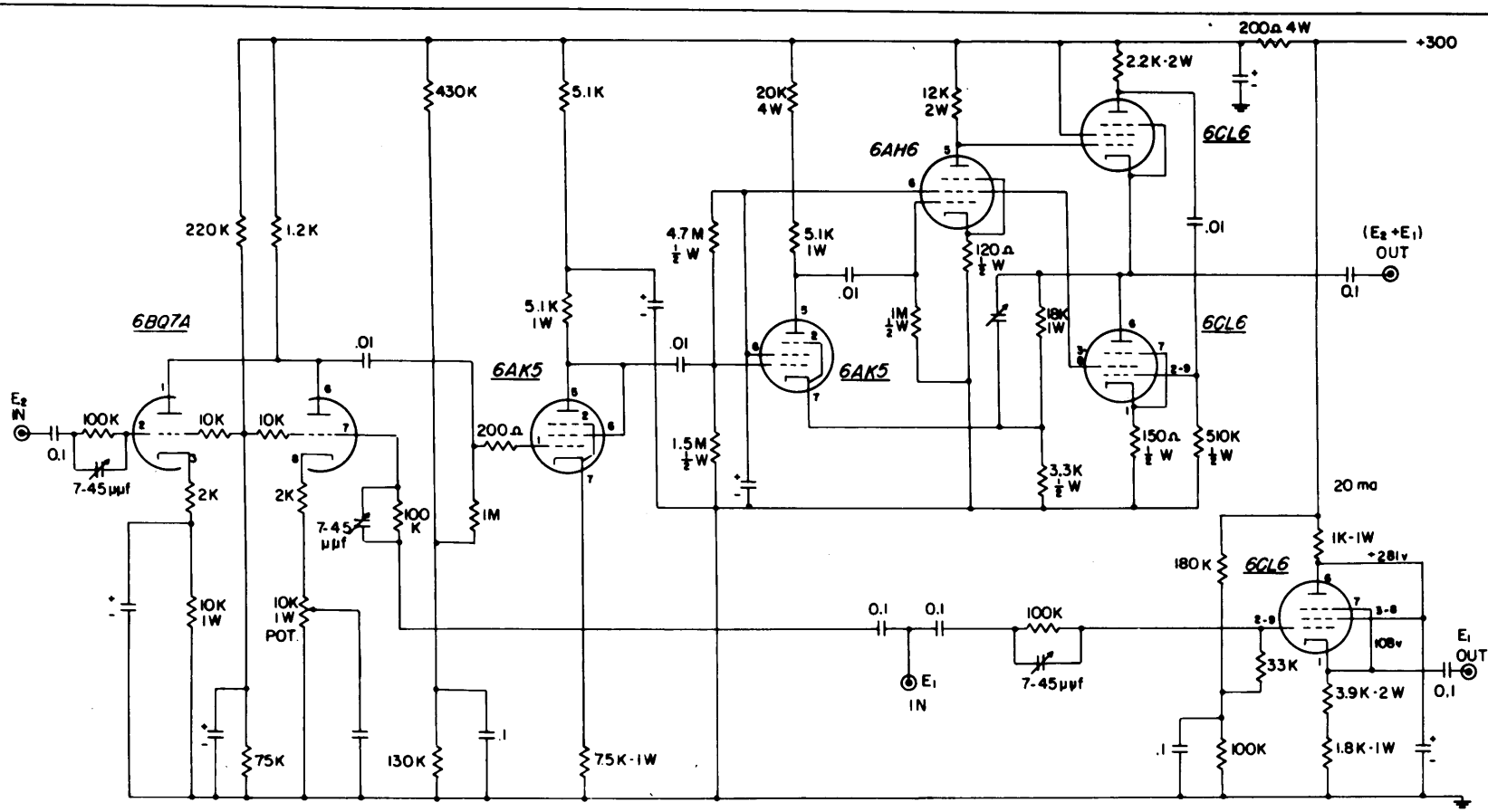

Figure 7. PULSE ADDER

are such that the pulses appearing at the plate are proportional to the product of the pulses fed into the two grids over a 2-1/2 volt range. The additional 6BN6 tubes are provided to increase the multiplying range to 12-1/2 volts (see Figure 8). This multiplier circuit is a slight extension of a multiplier designed by C. W. Johnstone of Los Alamos, having a 5 x 5 array of 6BN6 tubes for multiplying instead of the 3 x 4 array originally used by Johnstone (J1). The use of a 5 x 5 array was suggested by Johnstone.

A quick check on the performance of the pulse multiplier was obtained by feeding the same pulses in both inputs and measuring the output as a function of the input. Figure 6 shows a time-exposure photograph of the oscilloscope when the input to the multiplier was displayed on the X axis of the oscilloscope and the output was displayed on the Y axis. The intensity grid was triggered when the pulses on the two axes were at their maxima. The trace was obtained by varying the input pulses continuously. The trace has bumps at the points where the range of pulse heights increases to include another row of 6BN6 tubes. These bumps occur because the cutoff and saturation voltages of 6BN6 tubes are not sharp. The variations of the trace from the curve $y = cx^2$ is less than 15 percent. Because the multiplier output is used only to identify particles, this performance is quite satisfactory. This result was obtained after the circuit was in operation for 8 months. When the circuit was first put into operation, a variation from the curve $y = cx^2$ of less than 6 percent was obtained (A1). At that time, a new set of 6BN6 tubes

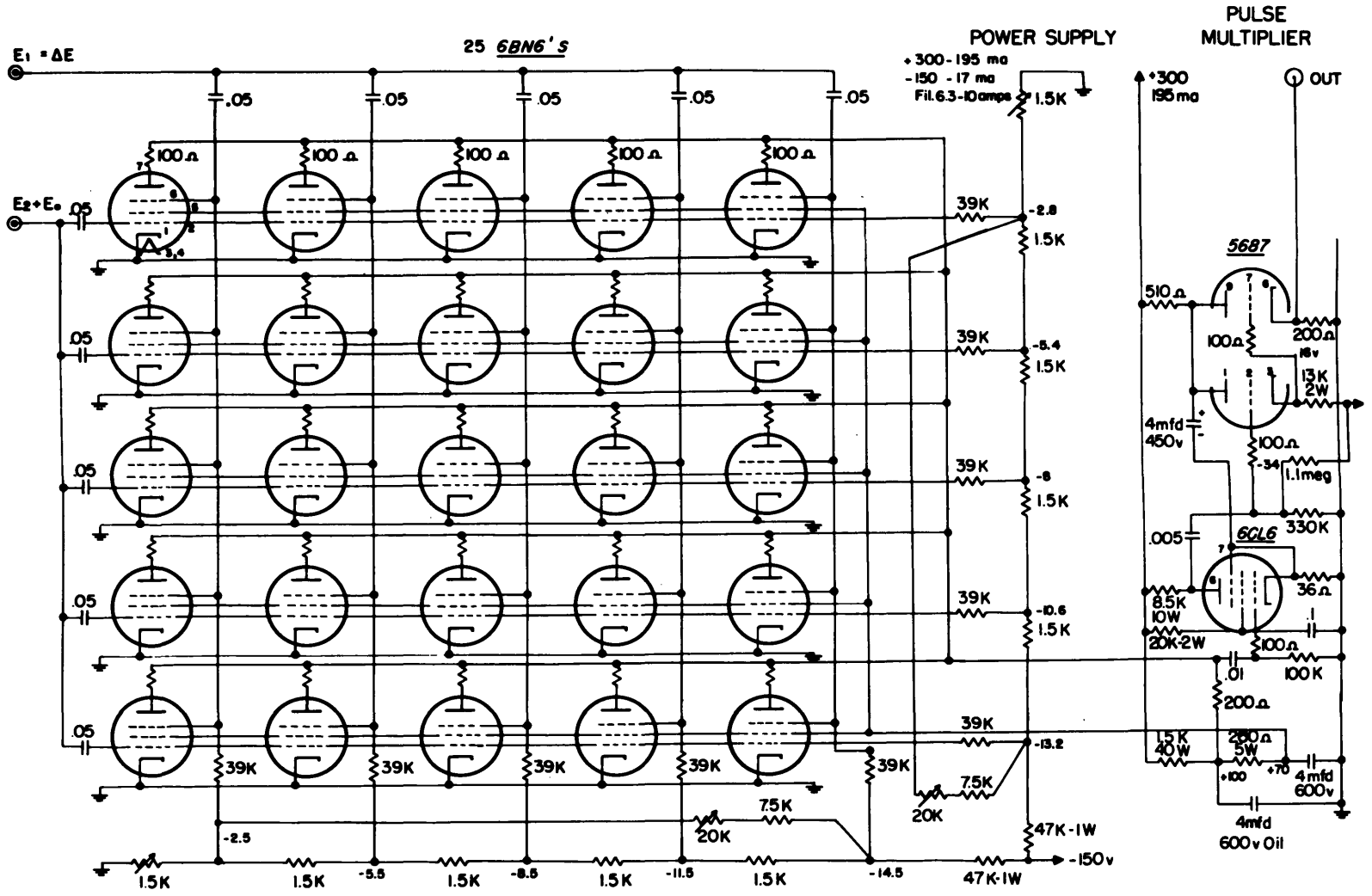

Figure 8

PULSE MULTIPLIER

was installed, which was carefully selected for uniform characteristics.

Figure 5(c) shows the pulse shape obtained from the pulse multiplier when the input pulses have the shapes shown in Figure 5(b).

4. Pulse Height Analyzers. The pulse height analyzers are single-channel pulse height analyzers of the same design as reported by Johnstone (J2), except for a minor change that makes the output pulses appear 0.5 μsec instead of 3 μsec after the triggering of the 6BN6 trigger tubes.

5. Coincidence Circuit. The coincidence circuit is used to register as coincidence counts pulses coming from the pulse height analyzers which result from pulses occurring simultaneously at the inputs of the analyzers. The pulses coming from the analyzers occur after the input pulses, depending upon the bias setting of the analyzers with respect to the input pulse heights. Therefore, to be certain that all true coincidences can be counted, it is necessary to use a coincidence circuit with a resolving time of approximately 3 μsec (see Figure 9).

The coincidences are not only counted electronically, but they are also used for triggering the Schmitt Trigger Circuit that turns on the intensity in the oscilloscope. Since it is necessary to turn on the intensity in the oscilloscope for very short times, the output stage of the coincidence circuit is designed to produce uniform pulses with very sharp peaks.

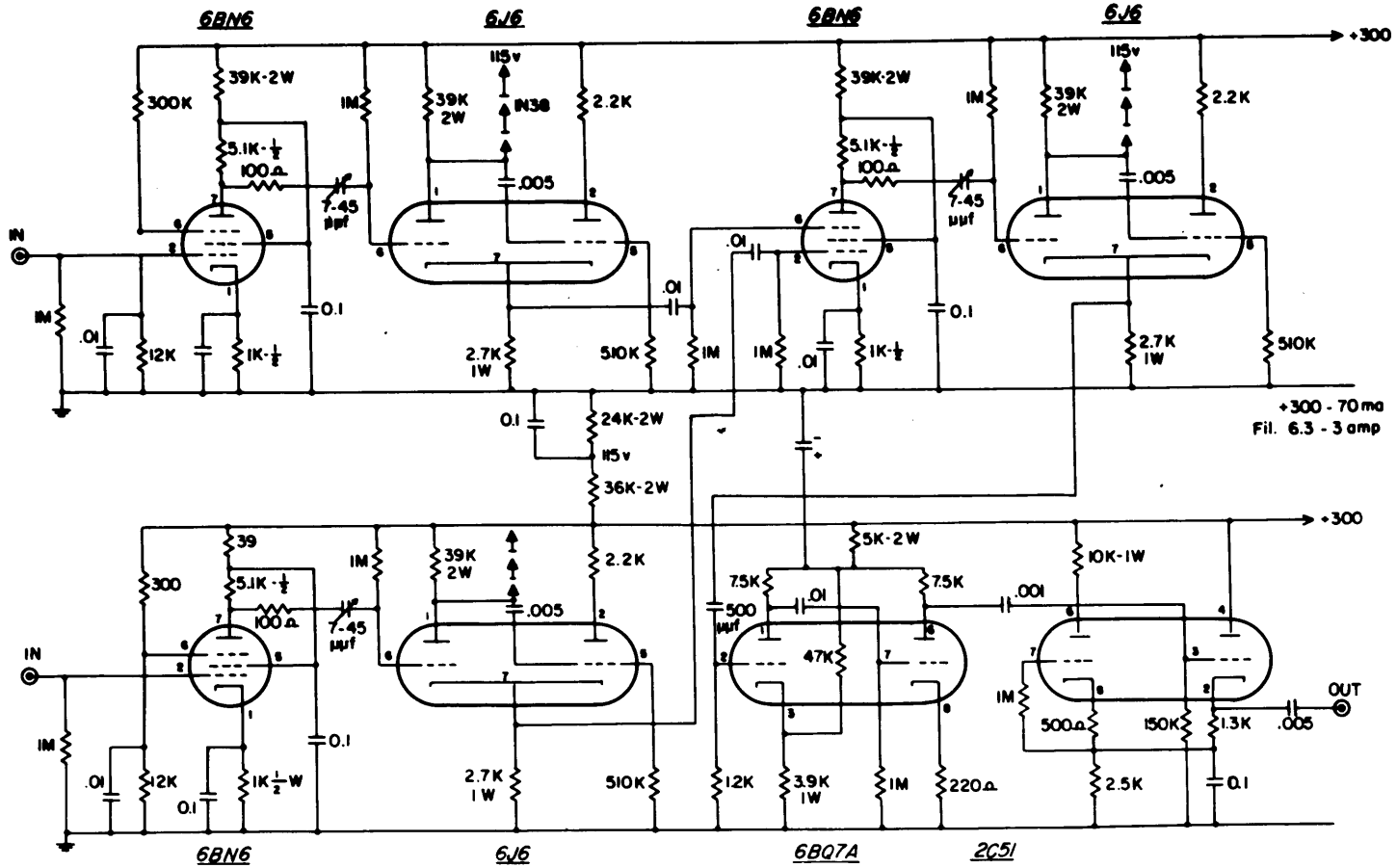

Figure 9. COINCIDENCE CIRCUIT

6. Oscilloscope. To provide spots of a very short time duration with sufficient intensity for observation and photographing, it is necessary to use a high-voltage cathode-ray tube. The tube used for this purpose is a Dumont Type 5RP-11A.

The oscilloscope amplifiers, which were designed by H. S. Stoddart, have a rise time of approximately 1/30 μsec (see Figure 10).

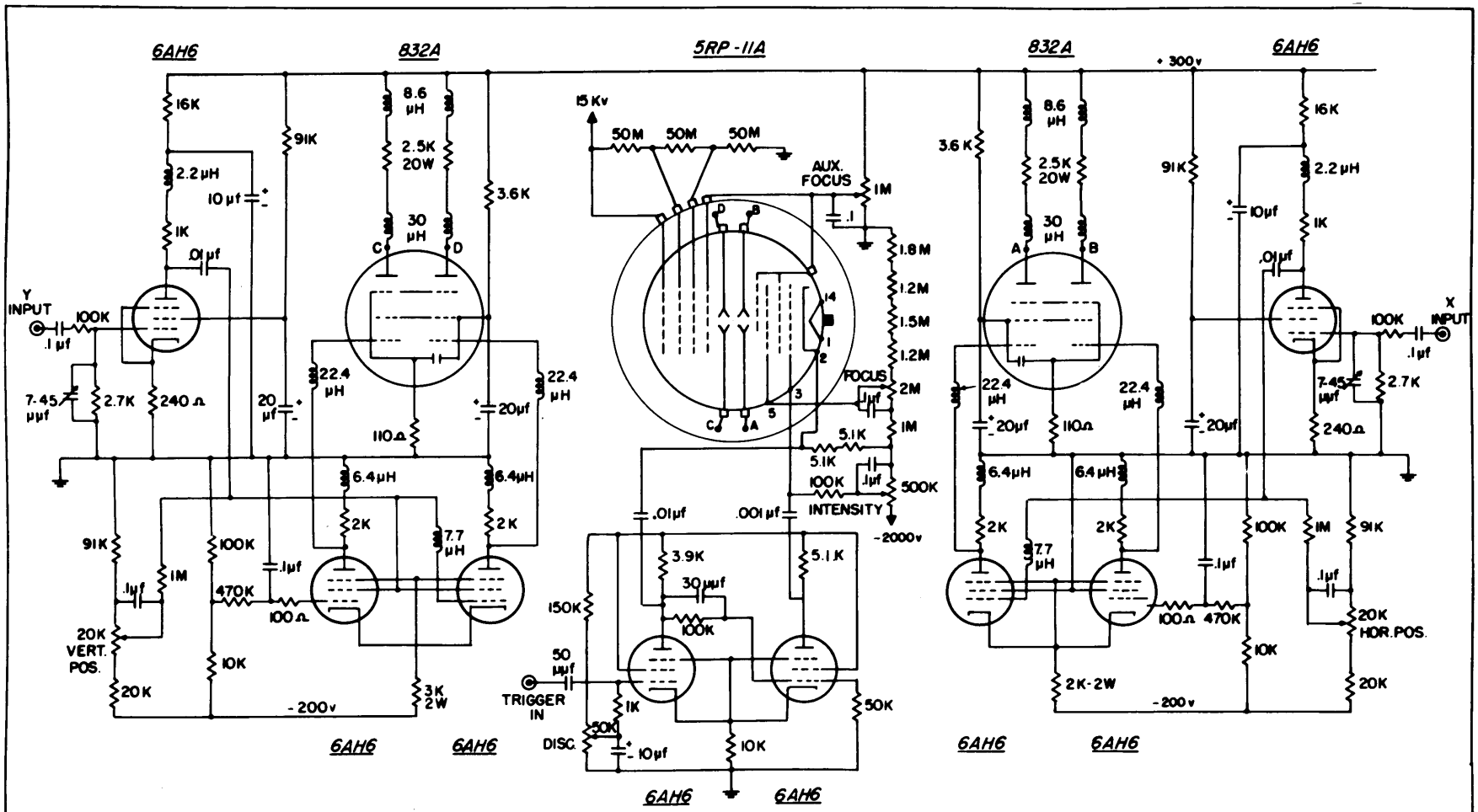

Figure 10. OSCILLOSCOPE

III. EXPERIMENTAL PROCEDURE

A. PARTICLE-SELECTION TECHNIQUE

Separated particle energy groups can readily be identified and measured using an oscilloscope-display system in conjunction with the particle selective counter. The procedure that can be used is as follows:

The output pulses from the two scintillation counters are shaped so that they have flat tops, and then they are displayed on the two axes of an oscilloscope. The pulses from each of the scintillation counters are also sent through two very stable single-channel analyzers and a coincidence circuit. The coincidence in time is used to trigger a Schmitt trigger circuit whose output pulse is applied to the intensity grid of the oscilloscope. The delay of the coincidence pulse is arranged so that it intensifies the beam of the oscilloscope only when the pulses displayed on the two axes are at their maxima. This results in a small spot appearing on the screen of the oscilloscope. The position of this spot shows the amplitudes of the two pulses coming from the two counters.

Figure 12(a) shows a time-exposure photograph of the oscilloscope screen with the particle selective counter observing the reaction particles from an oxidized Be^9 target bombarded with 15-Mev deuterons at an angle of 45 degrees from the incident deuteron beam. The output from the thin plastic scintillation counter is displayed on the X-axis and the output from the NaI(Tl) scintillation counter

is displayed on the Y-axis. The photograph shows separated lines representing the resolved particles of different mass and also individual particle energy groups. A similar photograph was presented in the November 30, 1953 issue of the Laboratory for Nuclear Science Progress Report (A2) showing the same target observed at an angle of 35 degrees from the incident deuteron beam. In this Progress Report a sketch is also presented showing the identification of some of the particle energy groups.

From the photograph in Figure 12(a), one can identify four separated proton groups and a continuum of protons all falling on a smooth curve at the left. One can also observe a doublet deuteron group and a continuum of deuterons all falling on a smooth curve next to the proton curve. The doublet deuteron group is due to the elastic deuterons from O^{16} and Be^{9}. The center-of-mass effect causes the elastic deuterons from Be^{9} to have lower energies than those from O^{16}. The photograph also shows the separated triton group from the reaction $Be^{9}(d,t)Be^{8}$ at the upper right. The spot at the lower left is the point of zero deflection.

For the groups that are well separated, one can visually adjust the bias and window width of each of the single-channel analyzers so that only the spot corresponding to the group desired remains on the oscilloscope screen. The intensity of this spot can then be measured by feeding the coincidence pulses into a scaler. Figure 12(b) shows a photograph of the oscilloscope screen when the pulse height

analyzers are adjusted to count the tritons from the reaction $Be^9(d,t)Be^8$. Figure 12(c) shows the same thing when the analyzers are adjusted to count the protons from the $Be^9(d,p)Be^{10}$ reaction.

There is a theoretical quantum-mechanical relationship which predicts dE/dx caused by collision processes. As given by Livingston and Bethe (L2), this relationship is

$$(dE/dx)_c = -(4\pi e^2 z^2 N/m v^2) \left\{ Z \left[\log_e(2m v^2/I) - \log_e(1 - v^2/c^2) - v^2/c^2 \right] - C_k \right\},$$

where:

z is the charge of the particles;

v is the velocity of the particles;

e is the charge on the electron;

m is the mass of the electron;

N is the atomic density of the absorber;

Z is the effective nuclear charge of the absorber;

I is the effective ionization potential of the absorber;

c is the velocity of light;

C_k is a correction term unimportant at high speeds.

For nonrelativistic particles, the above expression reduces to

$$(dE/dx)_c = K z^2/v^2,$$

where K varies only slightly with energy. Thus, the product $E(dE/dx)$ for nonrelativistic particles is approximately $C\ z^2\ M$, where C is a constant and M is the mass.

In the case of the particle selective counter, the particles lose an appreciable amount of energy in the plastic scintillator which is used to measure dE/dx. Therefore, the product $E_1 \cdot E_2$, where E_1 is the energy loss in the plastic scintillator and E_2 is the energy loss in the NaI(Tl) crystal, is not proportional to $z^2\ M$. Calculations from range-energy curves show that the product $E \cdot E_1$, where $E = E_1 + E_2$, is a constant proportional to the mass for protons in the region 5 to 20 Mev, for deuterons in the region 7 to 20 Mev, and for tritons in the region 9 to 20 Mev. The products for protons, deuterons, and tritons have ratios 1:1.8:2.6.

Figure 11 shows a block diagram of the electronic apparatus used when the product $E \cdot E_1$ is used to identify the mass of the reaction particles. The pulses from the two scintillation counters are first added electronically and then fed into one input of the pulse multiplier, while at the same time feeding the pulses from the plastic scintillator into the other input. The output from the pulse multiplier is then displayed on the X-axis of the oscilloscope, and the output from the NaI(Tl) scintillation counter is displayed on the Y-axis. The relative gains of the pulses are then adjusted to make the protons appear on a straight line. Figure 13(a) is a time-exposure photograph of the oscilloscope screen with the particle selective

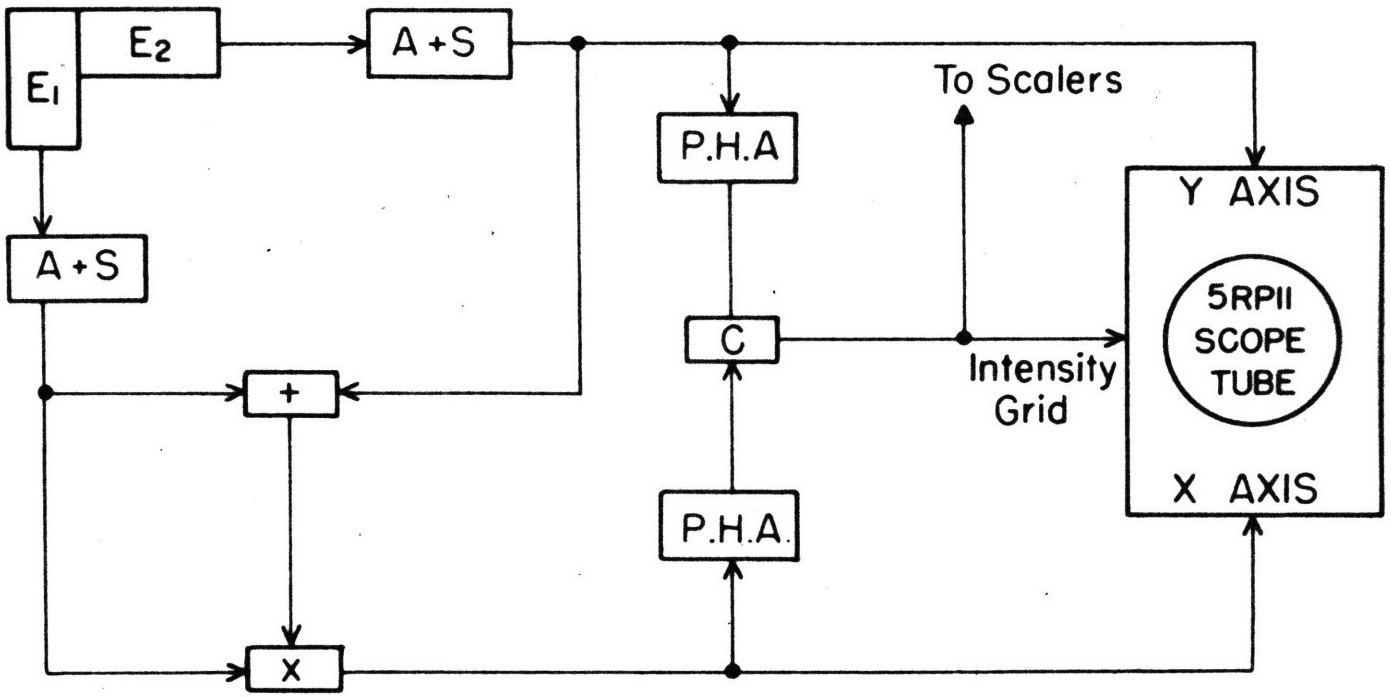

E_1 THIN PLASTIC SCINTILLATION COUNTER

E_2 NaI (Tl) SCINTILLATION COUNTER

A+S PULSE AMPLIFIER and SHAPER

P.H.A. PULSE HEIGHT ANALYZER

X PULSE MULTIPLIER

\+ PULSE ADDER

C COINCIDENCE CIRCUIT

Figure 11

BLOCK DIAGRAM OF APPARATUS

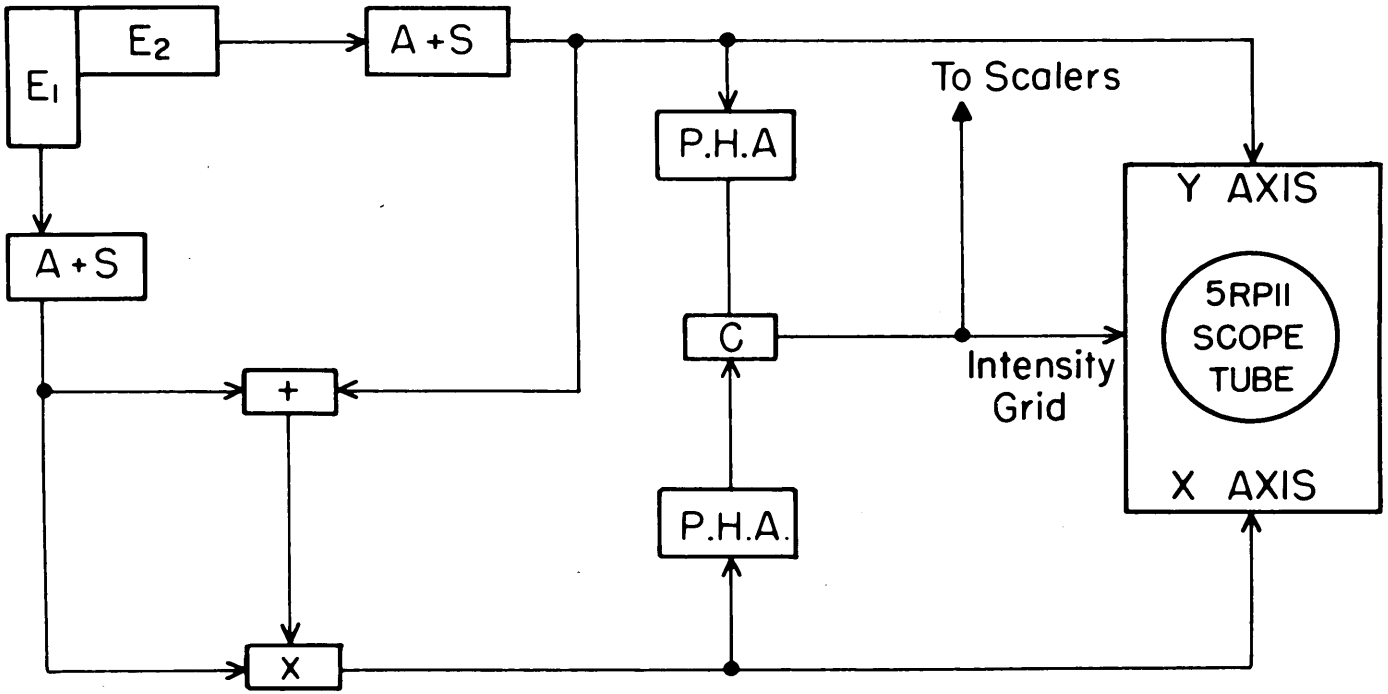

E_1 THIN PLASTIC SCINTILLATION COUNTER

E_2 NaI (Tl) SCINTILLATION COUNTER

A+S PULSE AMPLIFIER and SHAPER

P.H.A. PULSE HEIGHT ANALYZER

X PULSE MULTIPLIER

\+ PULSE ADDER

C COINCIDENCE CIRCUIT

BLOCK DIAGRAM OF APPARATUS

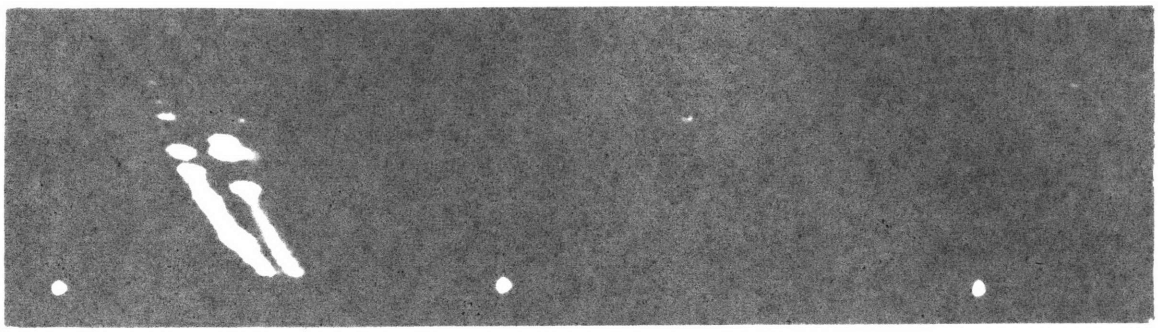

(a) (b) (c)

Figure 12. Photograph of oscilloscope screen when counter is observing oxidized Be target at 45 degrees from incident deuteron beam. Beam energy is approximately 15 Mev. E_1 displayed on X-axis, E_2 displayed on Y-axis. (a) Analyzers adjusted to count all particles. (b) Analyzers adjusted to count tritons from $Be^9(d,t)Be^8$ reaction. (c) Analyzers adjusted to count protons from $Be^9(d,p)Be^{10}$ reaction.

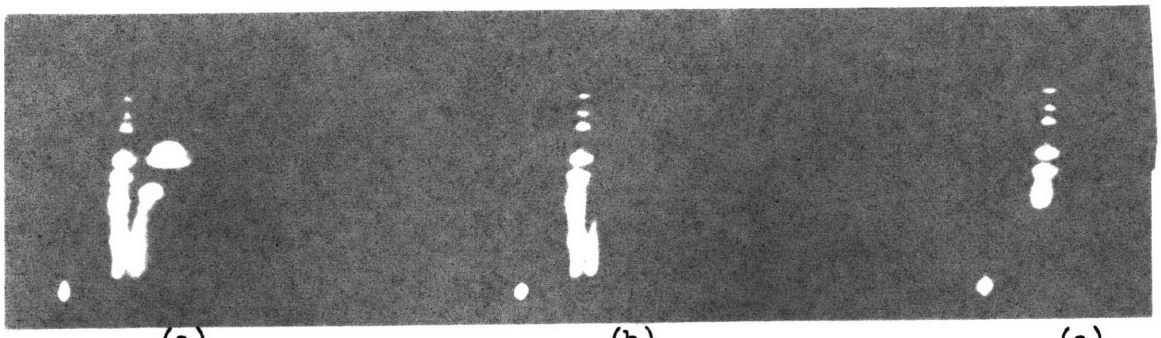

(a) (b) (c)

Figure 13. Photograph of oscilloscope screen when counter is observing oxidized Be target at 45 degrees from incident deuteron beam. Beam energy is approximately 15 Mev. Multiplier output displayed on X-axis, E_2 displayed on Y-axis. (a) Analyzers adjusted to count all particles. (b) Product analyzer adjusted to count protons. Some low-energy deuterons are leaking through. (c) Analyzers adjusted to count only protons. This shows the part of the proton spectrum that can be measured with only one adjustment of the product analyzer.

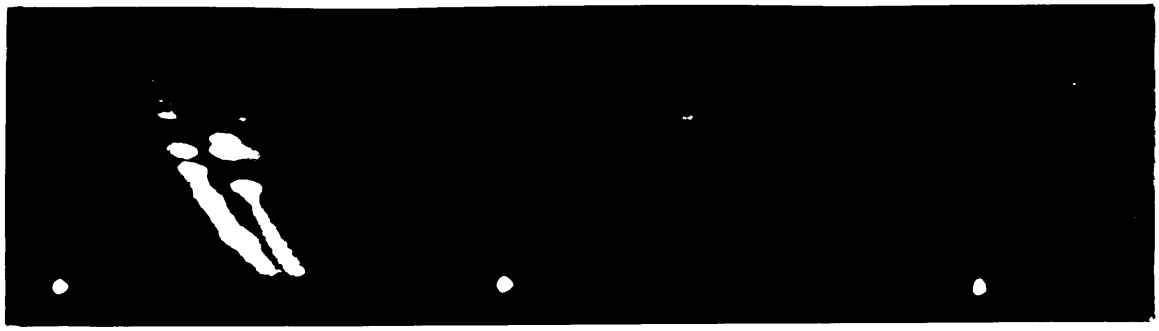

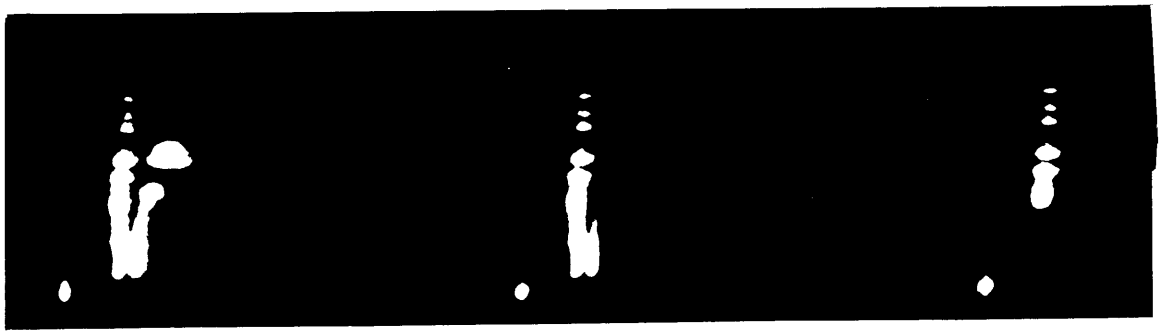

counter observing the reaction particles from the oxidized Be^9 target bombarded with 15-Mev deuterons at an angle of 45 degrees from the incident deuteron beam. The deviation of the deuteron spots from a straight line is believed to be due to the nonlinear response of the plastic scintillator to particles of high dE/dx.

The advantage of using the product $E \cdot E_1$ to identify the reaction particles is that a large part of the energy spectrum can be observed with the E_2 pulse height analyzer while using only one adjustment of the product analyzer. This is demonstrated in Figures 13(b) and 13(c).

When bombarding targets of high atomic number, no low-energy deuterons are observed. In these cases, a pulse height analysis of the entire proton energy spectrum can be made using only one adjustment of the product analyzer. Figures 14 and 15 show two examples. Figure 14(a) shows all the reaction particles emitted at 90 degrees when U^{238} is bombarded with 15-Mev deuterons. Figure 14(b) shows the same thing when the bias and window width of the product analyzer is adjusted to count protons only. Figures 15(b) and 15(a) show the same thing when Pb^{206} is bombarded with 15-Mev deuterons.

The human eye does not integrate well the light flashes on the oscilloscope screen. Therefore, time-exposure photographs of the oscilloscope screen are made with a Polaroid Land Camera to determine whether or not the visual adjustments of the amplifier gains and the bias and window widths are correct.

(a) (b) (c)

Figure 16. Photograph of oscilloscope screen when counter is observing C^{12} H^1 target bombarded with 15-Mev deuterons. Multiplier output displayed on X-axis, E_2 displayed on Y-axis. (a) Counter angle 60 degrees. (b) Counter angle 45 degrees. Recoil proton group from $H^1(d,d)H^1$ just below inelastic deuteron group. (c) Counter angle 35 degrees. Recoil proton group from $H^1(d,d)H^1$ just above inelastic deuteron group.

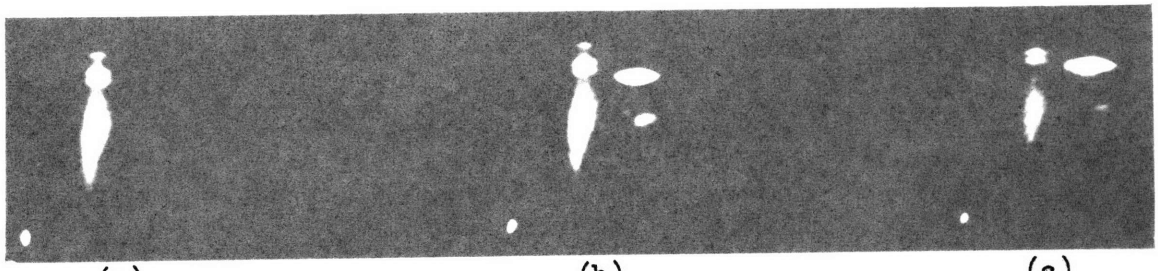

(a) (b) (c)

Figure 15. Photograph of oscilloscope screen when counter is observing Pb^{206} target bombarded with 15-Mev deuterons. Multiplier output displayed on X-axis, E_2 displayed on Y-axis. (a) Counter angle 90 degrees. Product analyzer adjusted for protons. (b) Counter angle 90 degrees. Analyzers adjusted for all particles. (c) Counter angle 60 degrees. Analyzers adjusted for all particles.

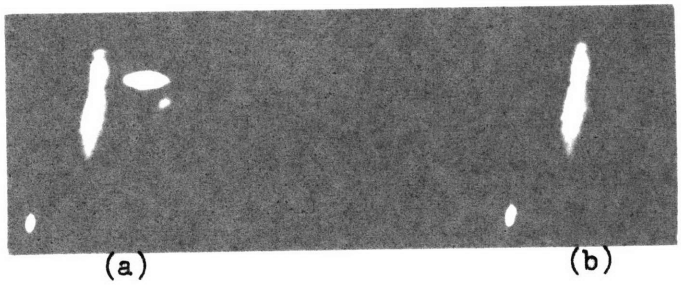

(a) (b)

Figure 14. Photograph of oscilloscope screen when counter is observing U^{238} target bombarded with 15-Mev deuterons. Counter angle 60 degrees. Multiplier output on X-axis, E_2 on Y-axis. (a) Analyzers adjusted for all particles. (b) Analyzers adjusted for protons.

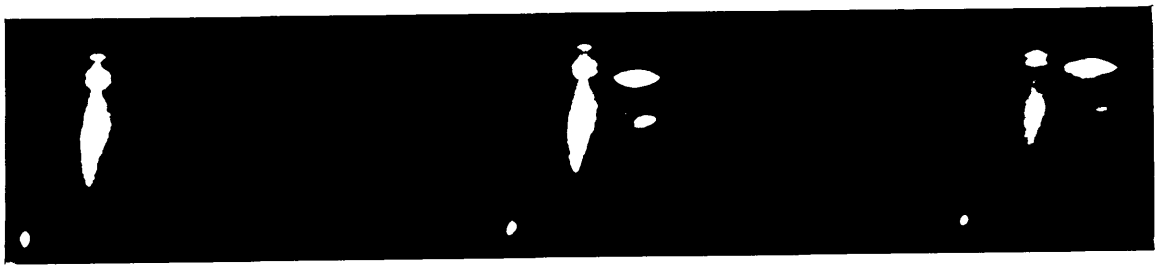

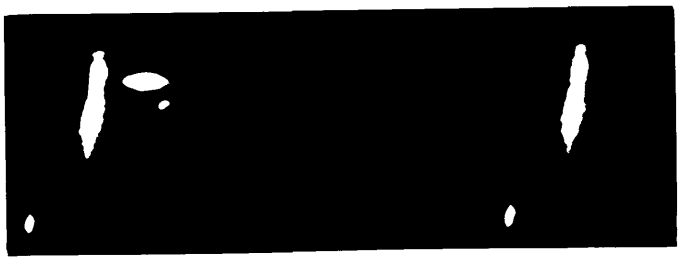

By photographing the oscilloscope screen, it is also possible to make a quick qualitative survey of each target. Some of the things that can be quickly observed are:

1. Because of the center-of-mass effect, oxygen and hydrogen contaminations can quickly be observed. Figure 12(a) shows the doublet elastic deuteron group observed when an oxidized Be^9 target is bombarded with 15-Mev deuterons. Figure 16 shows how hydrogen contamination can be detected by observing the recoil protons from the $H^1(d,d)H^1$ reaction.

2. By examining the size and intensity of the spots on the photograph, a rough idea of the relative intensities of the particle groups can be obtained.

3. By taking pictures with the particle selective counter at several angles, a rough idea of the angular distributions can be obtained.

4. By taking a long exposure, low-intensity ground-state groups can be detected.

5. Several interesting features of the energy spectra can be immediately observed, as for example, the effect of the coulomb barrier on the lower parts of the spectra when observing targets of high atomic number (see Figures 14 and 15).

B. BEAM ENERGY MEASUREMENT AND ENERGY CALIBRATION

The method for determining the deuteron beam energy is the same as that described by Wall (W1). Briefly, this method is as follows:

A 2-mil thick polyethylene target is inserted in the beam at the center of the scattering chamber. A scintillation spectrometer (partially visible at the lower left of Figure 3) is used to observe the energy spectrum of the protons after they pass through a 217.7 mgs/cm^2 thick aluminum absorber at an angle of 45 degrees from the incident deuteron beam. The ratio E_p/E_p', where E_p and E_p' are the energies of the protons incident on the NaI(Tl) crystal from the reactions $C^{12}(d,p)C^{13}$ and $C^{12}(d,p')C^{13*}$, is determined by measuring the positions of the two highest-energy proton groups. Since E_p and E_p' depend upon the energy of incident deuterons, the ratio E_p/E_p' can be used to determine the deuteron beam energy.

After the deuteron beam energy is determined, the proton energy from the reaction $C^{12}(d,p)C^{13}$ is calculated; then with the help of range-energy curves, the energy of this proton group in the second counter (E_2) of the particle selective counter is determined. The position of the peak is also measured with the particle selective counter, which then determines E_2 as a function of pulse height.

The pulse height spectra are taken with a single-channel pulse height analyzer. A pulser, the output of which can be varied

linearly by a 10-turn precision (0.1 percent linearity) potentiometer from zero to 10 volts, is fed into the cathode follower adjacent to the photomultiplier that observes the flashes from the NaI(Tl) crystal. This pulser is used to calibrate the single-channel analyzer absolutely in such a way as to account for the window width and inherent bias, because zero bias on the analyzer does not correspond to zero pulse height.

After the E_2 spectrum of protons from an unknown target is measured with the particle selective counter, range-energy curves must again be consulted to determine the corresponding energies of the protons coming from the center of the target. Since the spectra measured in these experiments are continuous, curves showing E_p as a function of E_2 were prepared for each target. Figure 17 shows an example of such a curve.

C. CROSS-SECTION MEASUREMENTS

As pointed out in a previous section, the beam monitor consists of a scintillation spectrometer which observes particles scattered 45 degrees from the incident deuteron beam by a thin gold foil. The bias and window width of the monitor differential discriminator are adjusted so that it accepts only those pulses which are due to the particles with energies in the vicinity of the elastic deuterons. For incident deuteron beam energies between 10 and 15 Mev, over 97 percent of these particles are elastic deuterons. Previous measure-

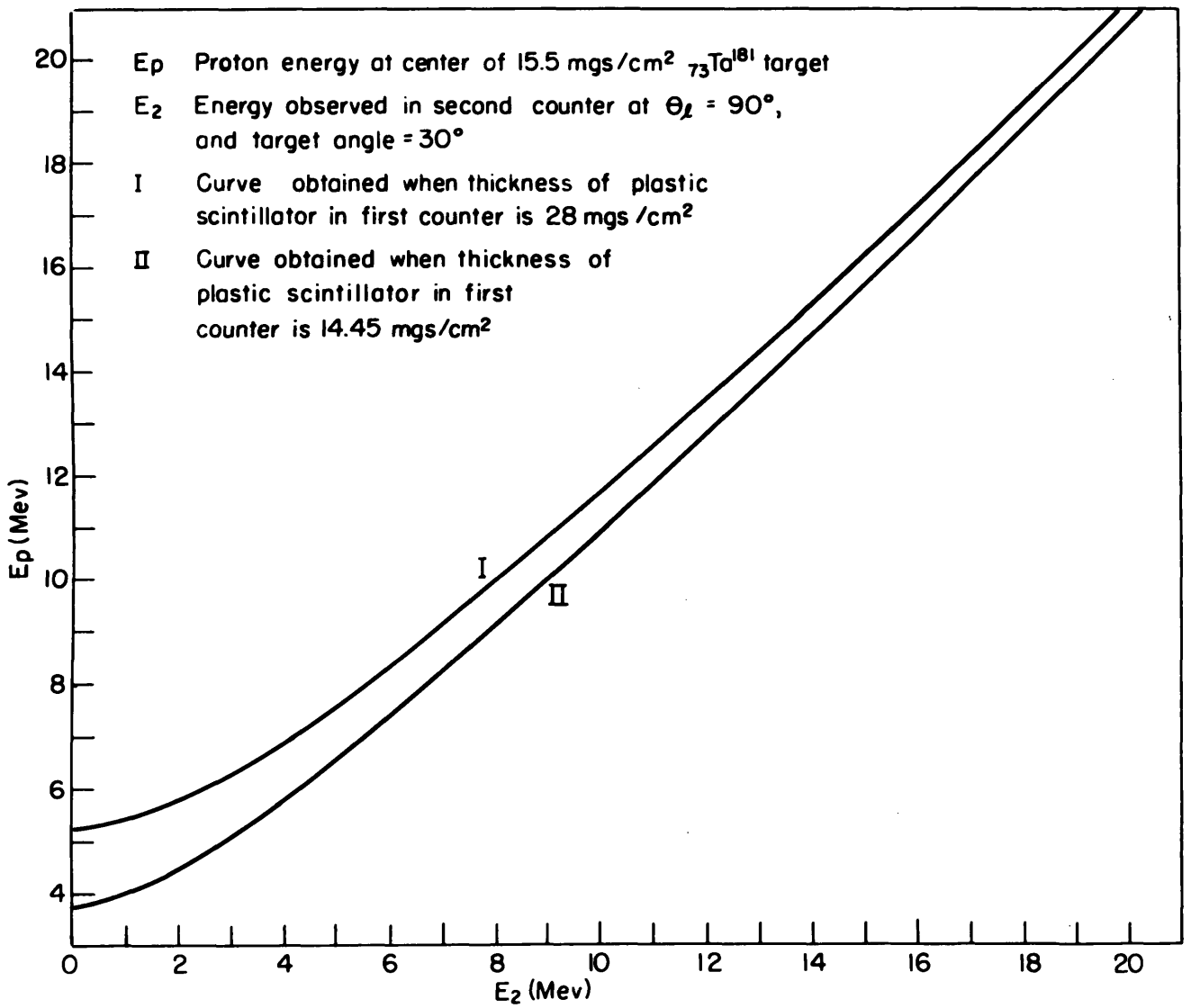
Ep Proton energy at center of 15.5 mgs/cm² $_{73}Ta^{181}$ target
E_2 Energy observed in second counter at θ_ℓ = 90°, and target angle = 30°
I Curve obtained when thickness of plastic scintillator in first counter is 28 mgs/cm²
II Curve obtained when thickness of plastic scintillator in first counter is 14.45 mgs/cm²
Ep (Mev)
E_2 (Mev)
I
II
0
2
4
6
8
10
12
14
16
18
20

Figure 17

ments of these cross sections agree within 10 percent with the cross sections calculated for Rutherford scattering (G2).

Since the beam monitor does not measure directly the deuteron beam, the differential cross sections were measured relative to a differential cross section that was previously measured by three independent methods. This cross section is for protons from the reaction $Ta^{181}(d,p)Ta^{182}$ with Q -2.23 Mev at 90 degrees from a 14-Mev deuteron beam (G1). The differential cross sections can readily be expressed in terms of this standard.

$$\sigma = \frac{C/N}{C_s/N_s} \frac{A/T}{A_s/T_s} \frac{\cos\varphi}{\cos\varphi_s} \sigma_s$$

where:

σ = differential cross section in mbs/atom-steradian in laboratory system;

C = integral counts or area under the differential spectrum curve;

N = number of incident deuterons;

A = atomic weight of target;

T = thickness of target;

φ = angle normal of target makes with deuteron beam;

s = subscript denoting the same values for the standard measurement.

Assuming that the monitor counter counts only elastically scattered deuterons, then,

$$N \propto \frac{M/\Omega}{\sigma_e}$$

where:

M = number of monitor counts;

Ω = monitor counter solid angle;

σ_e = differential cross section for elastic deuterons.

Assuming further that the differential cross section for elastic deuterons is given by the Rutherford cross section, then,

$$\sigma_e \propto \frac{1}{E_d^2}$$

Or,

$$N \propto \frac{M E_d^2}{\Omega} \qquad \text{and} \qquad N_s \propto \frac{M E_{d_s}^2}{\Omega_s}$$

where E_d is the deuteron beam energy at the monitor counter.

The deuteron beam energy was reduced to 14 Mev for the standard measurement by inserting aluminum foils in the deuteron beam.

Total cross sections were obtained by integrating graphically the angular distribution of the differential cross sections. Since, however, extreme forward angles could not be measured, the values for total cross sections obtained are only approximate values.

D. EXPERIMENTAL UNCERTAINTIES

Only the sources of error that have an appreciable effect on the experimental data are discussed here. These are discussed with respect to their effect on the experimental measurements.

1. Errors in Particle Selection. The separation of the protons and deuterons from all of the targets, for which data are presented here, was quite good. Figures 14 and 15 show two examples. These photographs (Figures 14 and 15) give the impression that, with the proper adjustments of the product analyzer bias and window width, clean proton energy spectra are observed. This is a wrong impression. Because of the long resolving time required for the coincidence circuit, chance coincidences between γ-rays and protons are possible. However, these chance coincidences are appreciable only at the low end of the energy spectrum where the γ-ray intensity is high.

The γ-ray background in the scattering chamber was checked by observing the pulses in the second counter with the targets removed. It was found that the γ-ray intensity under 2 Mev was greater than the total proton intensity during most of the experiments. The effect of chance coincidences between these low-energy γ-rays and protons on the observed spectra was checked by comparing the E_2 spectra observed when a 28 mgs/cm^2 plastic scintillator was used in the first counter with the E_2 spectra observed when a 14.45 mgs/cm^2 plastic scintillator was used in the first counter (see Figures 23 and 27). Although this comparison did not make it possible to make

an exact correction to the observed spectra, it did establish the approximate shape and magnitude of the chance coincidence background.

2. Error in Energy Calibration. After careful consideration of all the sources of error, it is estimated that the E_2 (energy in second counter) calibrations are correct to within $\pm$ 250 kev at E_2 = 15 Mev and $\pm$ 50 kev at E_2 = 1 Mev. Checks on proton groups with previously measured Q-values indicate that, in most cases, the calibrations were considerably better than the values quoted here.

The inaccuracy in the E_p calibration is considerably different at low proton energies. This calibration is believed to be accurate to $\pm$ 350 kev at E_p = 6 Mev and $\pm$ 200 kev at E_p = 15 Mev. The reason for the difference is, at low proton energies, the calibration is almost directly dependent on the range-energy curves; whereas, at high proton energies, it is dependent only on the slope which is known considerably better.

The sources of error in the energy calibration are:

a. Error in thickness measurements of plastic scintillators and aluminum foils in the first counter.

The plastic scintillators and aluminum foils were weighed with a Model 1055 Voland Analytical Balance. The values obtained were then divided by the cross-sectional areas to determine the thickness in mgs/cm^2.

It is estimated that the thicknesses of the aluminum foils were determined to within ± 1 percent, but because the aluminum foils were much thinner than the plastic scintillators, this inaccuracy in thickness determination had a negligible effect on the energy calibration.

The thicknesses of the plastic scintillators were determined to within ± .4 percent. This inaccuracy is small when compared to the inaccuracy of the range-energy determination for the plastic material. The effect is at most ± 20 kev at E_p = 6 Mev and considerably less at E_p = 15 Mev.

b. Error in range-energy curves.

The range-energy curves used were those published by Aron et al (A3). These range-energy curves were determined in the following manner. The rate of energy loss was computed from the theoretical formula given by Livingston and Bethe (L2) and the range-energy values were determined by numerical integration of the reciprocal of the rate of energy loss with respect to the energy, with low-energy values being based on experimental rather than theoretical data.

The plastic scintillator consists of equal parts of carbon and hydrogen and a small percentage of activator. The range-energy values for this material were calculated from the combined information on hydrogen and carbon taken from Aron et al. The small percentage of activator was neglected in these calculations. Table I shows the range-energy values resulting from these calculations. Because of

the inaccuracies in these calculations, it is believed that the curve is only correct to within 5 percent at E_p = 5 Mev and 2 percent at E_p = 15 Mev. This constitutes an error of $\pm$ 150 kev at E_p = 5 Mev and a negligible error at E_p = 15 Mev in the final energy calibrations.

Since the aluminum foils were much thinner than the plastic scintillator, the inaccuracies in the aluminum range-energy curves are believed to have had a negligible effect on the energy calibration.

TABLE I

Calculated Ranges of Protons in the Plastic Scintillator

E in Mev	Range in mgs/cm^2
1	2.20
3	14.23
5	35.14
6	48.65
7	64.14
8	81.56
9	100.86
10	122.01
12	169.76
14	224.58
16	286.30
18	354.77
20	429.84

c. Nonlinear response of NaI crystals.

NaI has been shown to have a linear response to protons in the energy ranges used in these experiments (F1, T1) to within 2 percent. This is a small error as compared to those previously mentioned.

d. Error in Q-values.

As previously mentioned, the proton groups from the $C^{12}(d,p)C^{13}$ and $C^{12}(d,p')C^{13*}$ reactions were used for energy calibration. The Q-values for these reactions are quoted in the compilation by Ajzenberg and Lauritsen (A4). These values are probably known to within 10 kev; therefore, they add only a small error to the energy calibration.

e. Error in locating the center of the proton peaks.

The full width at half the maximum height of the $C^{12}(d,p)C^{13}$ proton peak was usually less than 300 kev. It was therefore possible to pick the maximum to within 30 kev.

f. Other effects.

Other effects that might introduce small systematic errors are incorrect determinations of counter angle and target angle. The counter angle is determined by a bridge network, one arm of which is a variable precision linear resistor connected to the arm carrying the counter. The zero is found by measuring elastically scattered deuterons on each side of zero degrees and finding the points on the

balancing variable resistor in the bridge which give equal intensities. In this way the angle can be determined to approximately 0.25 degrees. The target angle is determined in a similar way.

A slightly larger source of error is the inaccuracy of the target-stopping powers for low-energy protons. The target-stopping powers used were those determined by Harvey (H2). These stopping powers are given in mgs/cm^2 equivalent to 1 mg/cm^2 of aluminum for 19-Mev protons. This is not exactly a constant throughout the proton energy range, and therefore an error is introduced for low-energy protons.

g. Error in beam energy measurements.

The sources of error in the beam energy measurements were of the same nature as those described for the energy calibration of the second counter of the particle selective counter. The only difference is that the scintillation spectrometer used for the energy measurement had a 217.7 mgs/cm^2 aluminum absorber in front of the NaI(Tl) crystal instead of the plastic scintillator. It is estimated that the deuteron beam energies were measured to well within 200 kev. Since the measured beam energies were used for the energy calibrations of the second counter of the particle selective counter, the inaccuracies in beam energy determinations affected the energy calibrations directly.

3. Error in Cross-Section Measurements. As previously stated, the differential cross sections were measured relative to the differential cross section for $_{73}Ta^{181}(d,p)_{73}Ta^{182}$ reactions with $Q > -2.23$ Mev at an angle of 90 degrees from the incident deuteron beam. This differential cross section has been previously measured by Gove et al (G1). From the method used for this measurement, it is estimated that the value given is probably only correct to within 20 percent.

The accuracy of the relative differential cross-section measurements depend upon the accuracy of the target thickness determinations, the extent to which the monitor counter observed Rutherford scattered deuterons, and the saturation of the monitor counter caused by high counting rates.

Since the differential cross sections for extreme forward angles were not measured, the values quoted for the total cross sections can only be considered as rough estimates that are probably correct to only $\pm$ 40 percent, and in some cases they may be less accurate.

IV. EXPERIMENTAL DATA

$_{41}Nb^{93}$ (25.4 mgs/cm^2 metal foil)

The proton energy spectrum in the second counter was first observed using a 28 mgs/cm^2 thick plastic scintillator in the first counter. However, in this case a large part of the low-energy protons coming from the target was stopped in the first counter. Therefore, the experiment was repeated using a 14.45 mgs/cm^2 thick plastic scintillator in the first counter. Figure 18 shows the section of the spectrum observed in the latter case.

Since the resolution obtained with the 14.45 mgs/cm^2 plastic scintillator was not good enough to separate all the protons from the deuterons, no cross-section measurements were attempted.

$_{47}Ag^{107}$ ^{109} (7.25 mgs/cm metal foil of natural Ag; i.e., 51.4 percent Ag^{107} and 48.6 percent Ag^{109})

Figure 19 shows the proton energy spectrum observed in the second counter at a counter angle of 90 degrees. The spectrum was also observed at 30, 45, 60, and 120 degrees. Figure 20 shows separate angular distributions for the protons with $Q < -2.23$ Mev and $Q > -2.23$ Mev.

The total cross sections were estimated by graphically integrating the angular distributions. The values obtained were 284 millibarns/atom for $Q < -2.23$ Mev and 100 millibarns/atom for $Q > -2.23$ Mev.

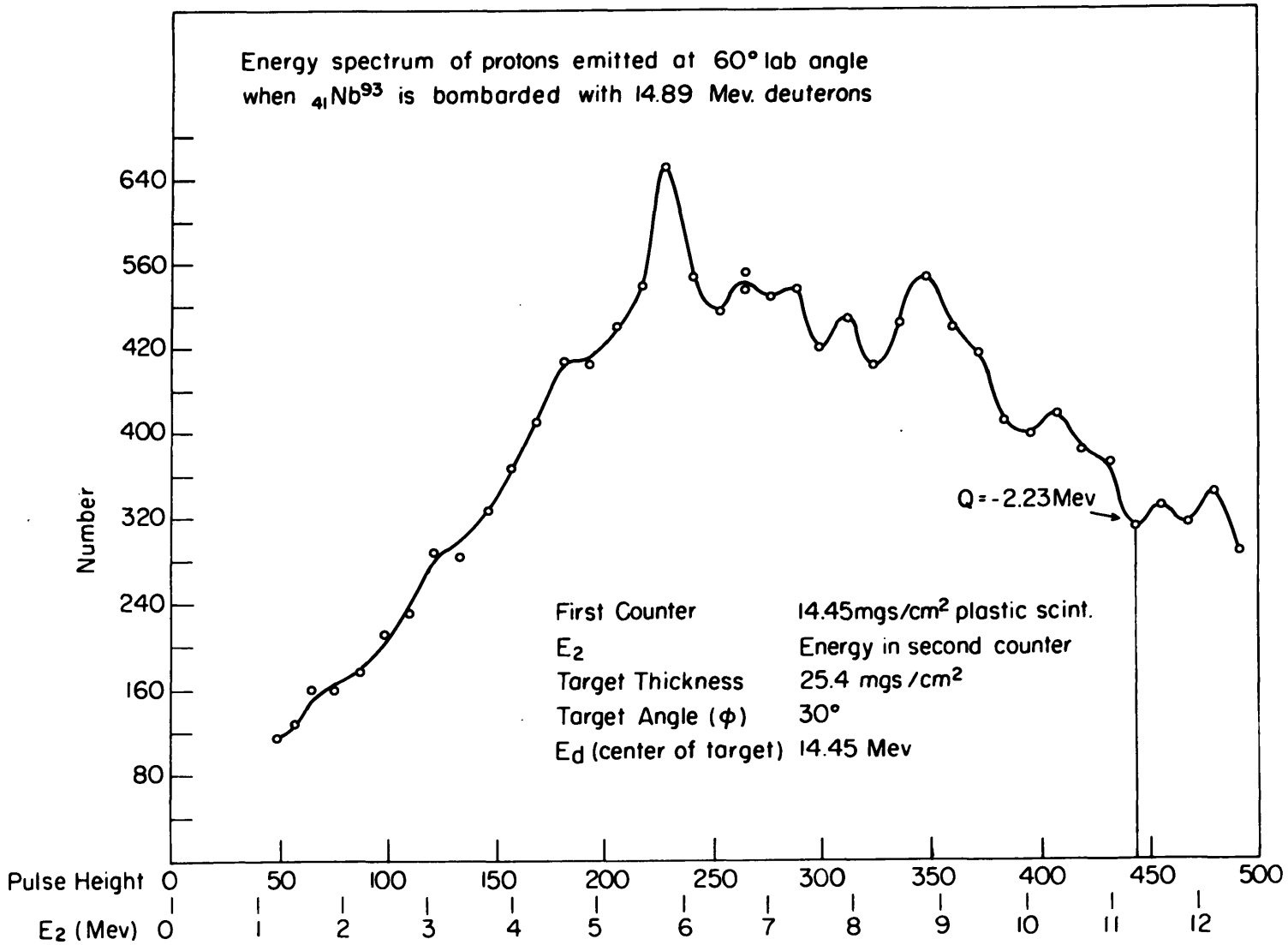
Energy spectrum of protons emitted at 60° lab angle
when $_{41}Nb^{93}$ is bombarded with 14.89 Mev. deuterons
Number
640
560
420
400
320
240
160
80
Q = -2.23Mev
First Counter 14.45mgs/cm² plastic scint.
E2 Energy in second counter
Target Thickness 25.4 mgs/cm²
Target Angle (φ) 30°
Ed (center of target) 14.45 Mev
Pulse Height 0 50 100 150 200 250 300 350 400 450 500
E2 (Mev) 0 1 2 3 4 5 6 7 8 9 10 11 12

Figure 18

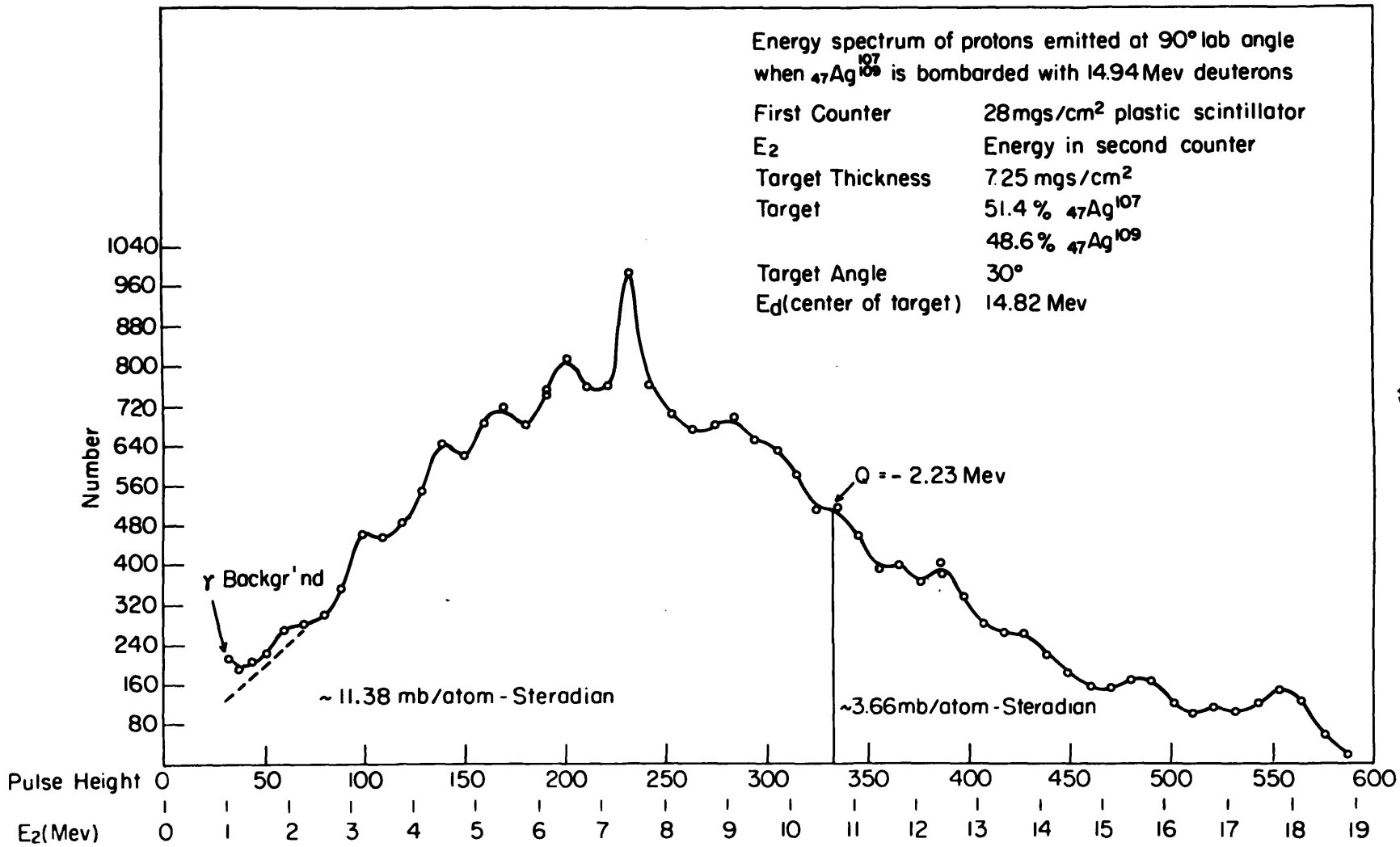
Energy spectrum of protons emitted at 90° lab angle
when $_{47}Ag^{107}$ is bombarded with 14.94 Mev deuterons
First Counter 28 mgs/cm² plastic scintillator
E2 Energy in second counter
Target Thickness 7.25 mgs/cm²
Target 51.4 % $_{47}Ag^{107}$
48.6 % $_{47}Ag^{109}$
Target Angle 30°
Ed(center of target) 14.82 Mev
Number
1040
960
880
800
720
640
560
480
400
320
240
160
80
γ Backgr'nd
Q = - 2.23 Mev
~ 11.38 mb/atom - Steradian
~3.66mb/atom - Steradian
Pulse Height 0 50 100 150 200 250 300 350 400 450 500 550 600
E2(Mev) 0 1 2 3 4 5 6 7 8 9 10 11 12 13 14 15 16 17 18 19

Figure 19

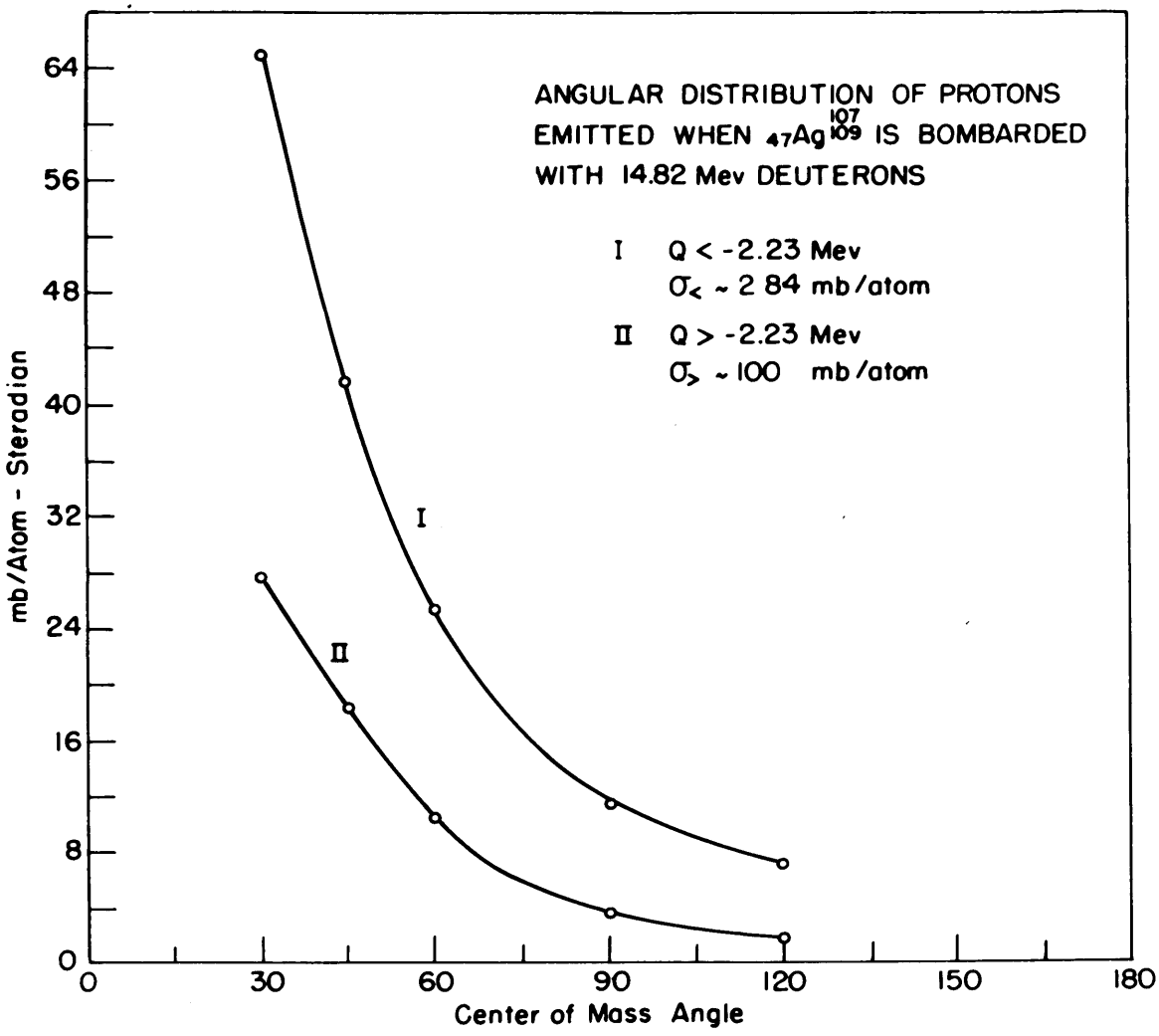
ANGULAR DISTRIBUTION OF PROTONS
EMITTED WHEN $_{47}Ag^{107}_{109}$ IS BOMBARDED
WITH 14.82 Mev DEUTERONS
I Q < -2.23 Mev
$\sigma_<$ ~ 2 84 mb/atom
II Q > -2.23 Mev
$\sigma_>$ ~ 100 mb/atom
I
II
mb/Atom - Steradian
0
8
16
24
32
40
48
56
64
0
30
60
90
120
150
180
Center of Mass Angle

Figure 20

$_{51}Sb^{121}$ $_{123}$ (4.8 mgs/cm^2 evaporated target of natural Sb; i.e., 57.2 percent Sb^{121} and 42.8 percent Sb^{123})

The proton energy spectrum observed in the second counter at an angle of 60 degrees is shown in Figure 21. The spectrum was also observed at counter angles of 45, 90, and 120 degrees. The separate angular distributions for $Q < -2.23$ Mev and $Q > -2.23$ Mev are almost identical in shape to that for Ag (see Figure 20).

The total cross sections were estimated to be 277 millibarns/atom for $Q < -2.23$ Mev and 128 millibarns/atom for $Q > -2.23$ Mev.

$_{73}Ta^{181}$ (15.5 mgs/cm^2 metal foil)

The proton energy spectra in the second counter were observed at counter angles of 45, 60, 75, 90, 120, and 150 degrees for several deuteron beam energies ranging from 10.84 to 14.75 Mev. Figures 22, 23, 24, 25, and 26 show the spectra observed at 90 degrees.

The angular distributions for each of the deuteron beam energies were found to be very similar, the only difference being that the angular distributions are slightly more forward for the higher deuteron energies. The angular distribution for $Q > -2.23$ Mev and a deuteron energy of 14 Mev has been previously measured by Gove et al (G1). The corresponding angular distribution for $Q < -2.23$ Mev is only slightly different from that for Pb^{207} (see Figure 30). The only difference is that the angular distribution for Ta rises more steeply at forward angles.

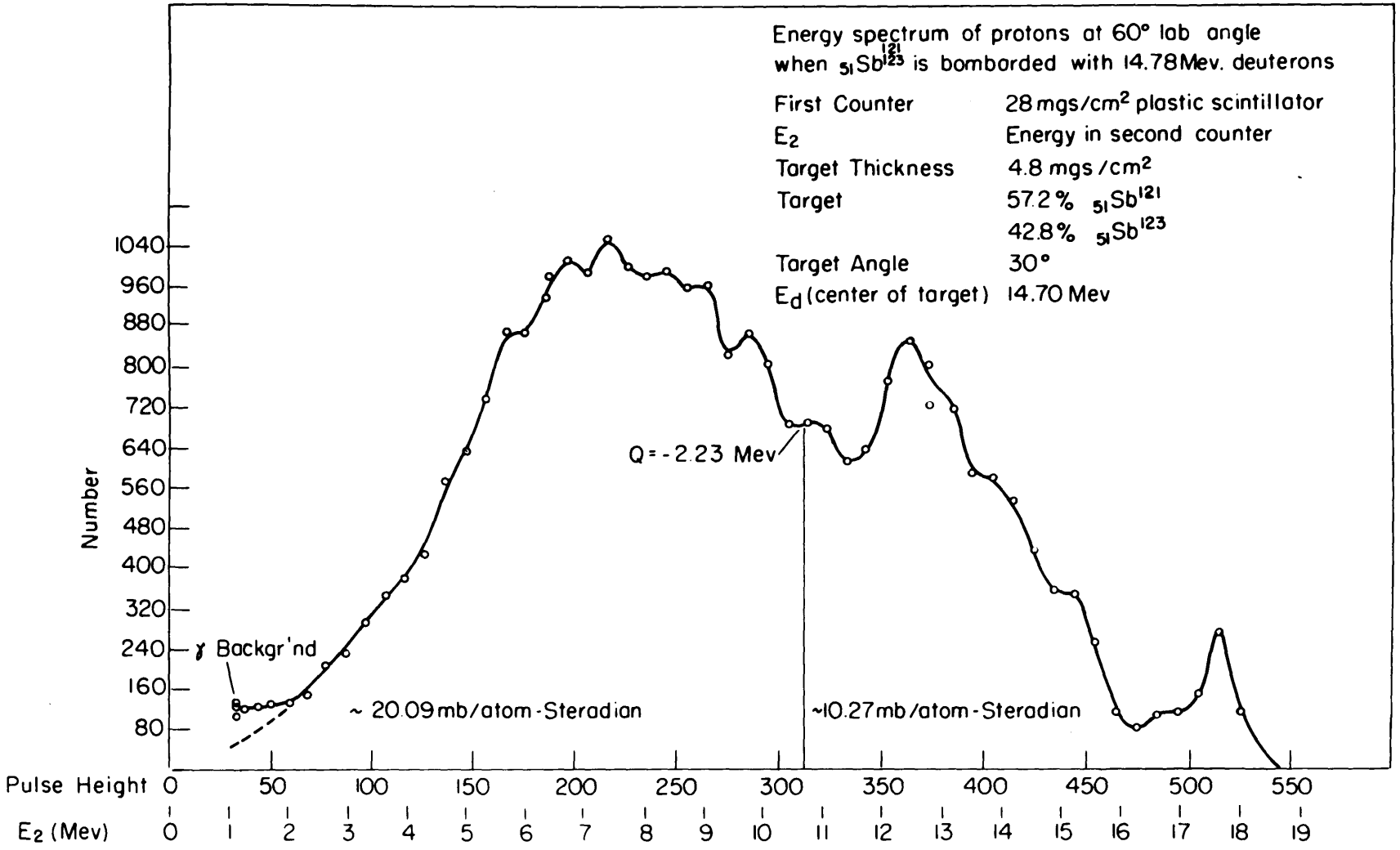
Energy spectrum of protons at 60° lab angle
when $_{51}Sb^{121}_{123}$ is bombarded with 14.78Mev. deuterons
First Counter 28 mgs/cm² plastic scintillator
E2 Energy in second counter
Target Thickness 4.8 mgs/cm²
Target 57.2% $_{51}Sb^{121}$
42.8% $_{51}Sb^{123}$
Target Angle 30°
Ed (center of target) 14.70 Mev
Number
1040
960
880
800
720
640
560
480
400
320
240
160
80
γ Backgr'nd
Q = -2.23 Mev
~ 20.09 mb/atom-Steradian
~10.27 mb/atom-Steradian
Pulse Height 0 50 100 150 200 250 300 350 400 450 500 550
E2 (Mev) 0 1 2 3 4 5 6 7 8 9 10 11 12 13 14 15 16 17 18 19

Figure 21

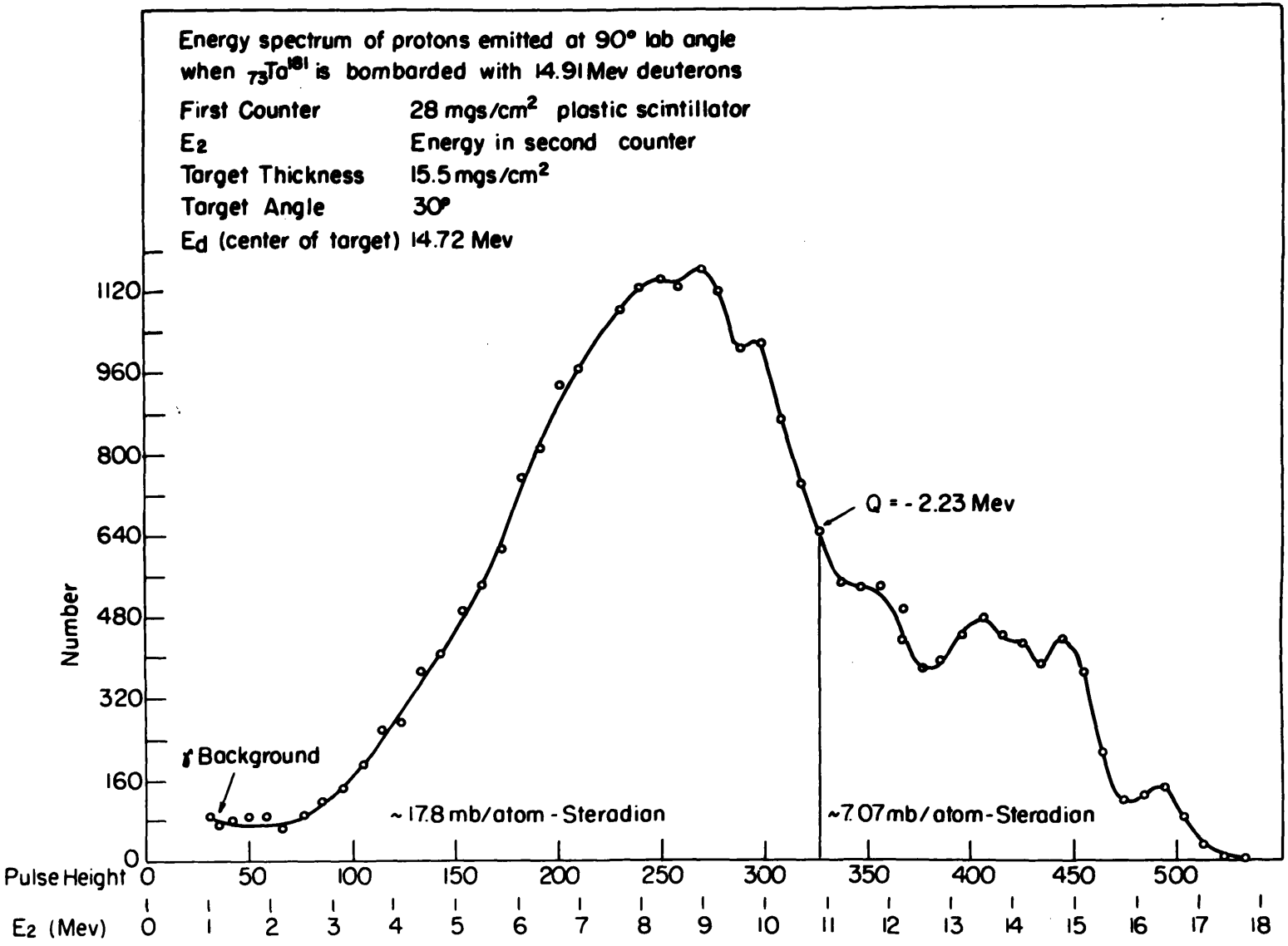
Energy spectrum of protons emitted at 90° lab angle
when $_{73}Ta^{181}$ is bombarded with 14.91 Mev deuterons
First Counter 28 mgs/cm² plastic scintillator
E2 Energy in second counter
Target Thickness 15.5 mgs/cm²
Target Angle 30°
Ed (center of target) 14.72 Mev
Number
1120
960
800
640
480
320
160
0
Q = - 2.23 Mev
Background
~ 17.8 mb/atom - Steradion
~7.07 mb/atom-Steradion
Pulse Height 0 50 100 150 200 250 300 350 400 450 500
E2 (Mev) 0 1 2 3 4 5 6 7 8 9 10 11 12 13 14 15 16 17 18

Figure 22

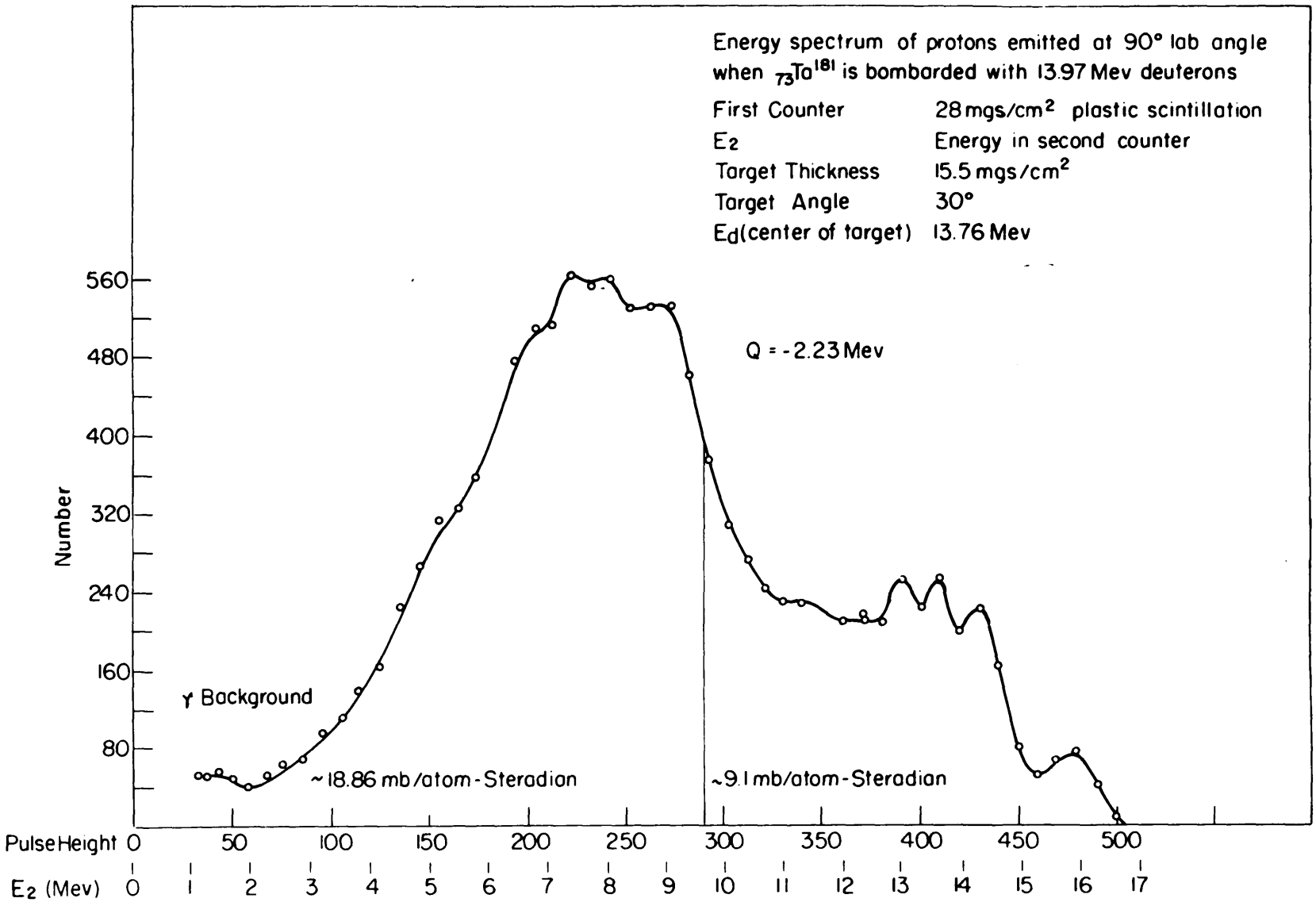
Energy spectrum of protons emitted at 90° lab angle
when $_{73}Ta^{181}$ is bombarded with 13.97 Mev deuterons
First Counter 28 mgs/cm² plastic scintillation
E2 Energy in second counter
Target Thickness 15.5 mgs/cm²
Target Angle 30°
Ed(center of target) 13.76 Mev
Q = -2.23 Mev
γ Background
~18.86 mb/atom-Steradian
~9.1 mb/atom-Steradian
Number
560
480
400
320
240
160
80
Pulse Height 0 50 100 150 200 250 300 350 400 450 500
E2 (Mev) 0 1 2 3 4 5 6 7 8 9 10 11 12 13 14 15 16 17

Figure 23

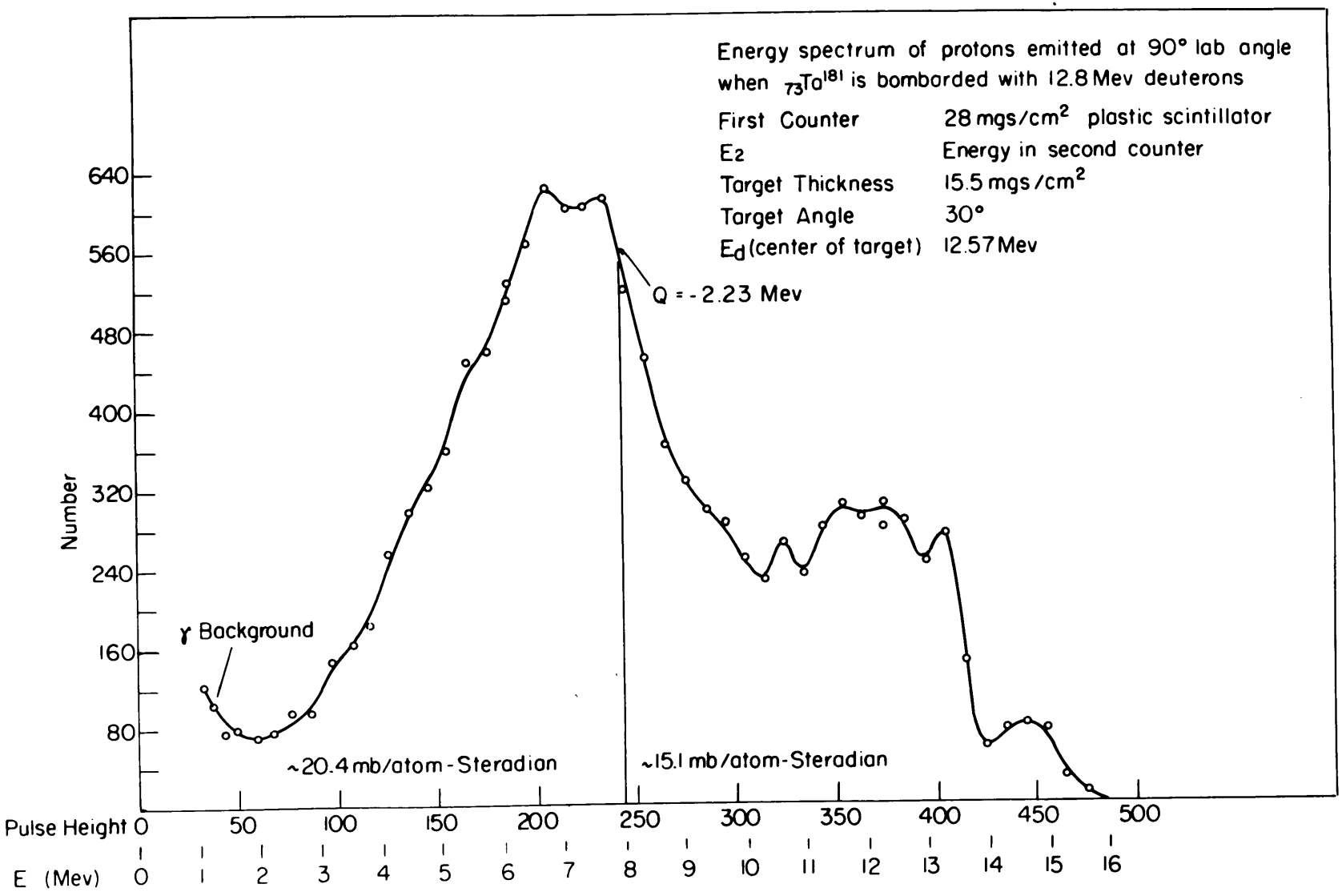
Energy spectrum of protons emitted at 90° lab angle
when $_{73}Ta^{181}$ is bombarded with 12.8 Mev deuterons
First Counter 28 mgs/cm² plastic scintillator
E2 Energy in second counter
Target Thickness 15.5 mgs/cm²
Target Angle 30°
Ed (center of target) 12.57 Mev
Q = -2.23 Mev
γ Background
~20.4 mb/atom - Steradian
~15.1 mb/atom - Steradian
Number
640
560
480
400
320
240
160
80
Pulse Height 0 50 100 150 200 250 300 350 400 450 500
E (Mev) 0 1 2 3 4 5 6 7 8 9 10 11 12 13 14 15 16

Figure 24

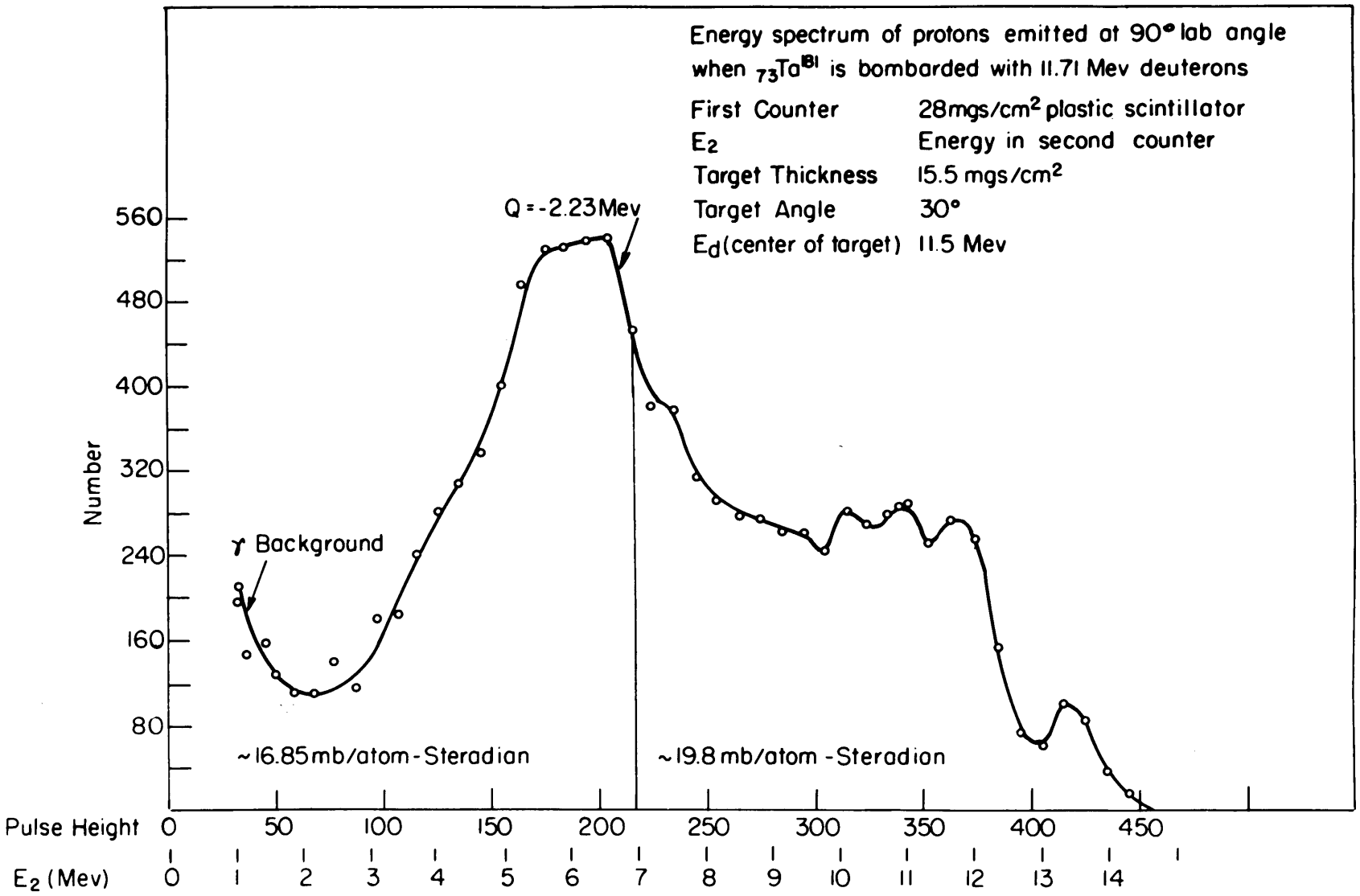
Energy spectrum of protons emitted at 90° lab angle
when $_{73}Ta^{181}$ is bombarded with 11.71 Mev deuterons
First Counter 28mgs/cm² plastic scintillator
E_2 Energy in second counter
Target Thickness 15.5 mgs/cm²
Target Angle 30°
E_d(center of target) 11.5 Mev
Q = -2.23Mev
γ Background
~16.85mb/atom-Steradian
~19.8 mb/atom -Steradian
Number
560
480
400
320
240
160
80
Pulse Height 0 50 100 150 200 250 300 350 400 450
E_2 (Mev) 0 1 2 3 4 5 6 7 8 9 10 11 12 13 14

Figure 25

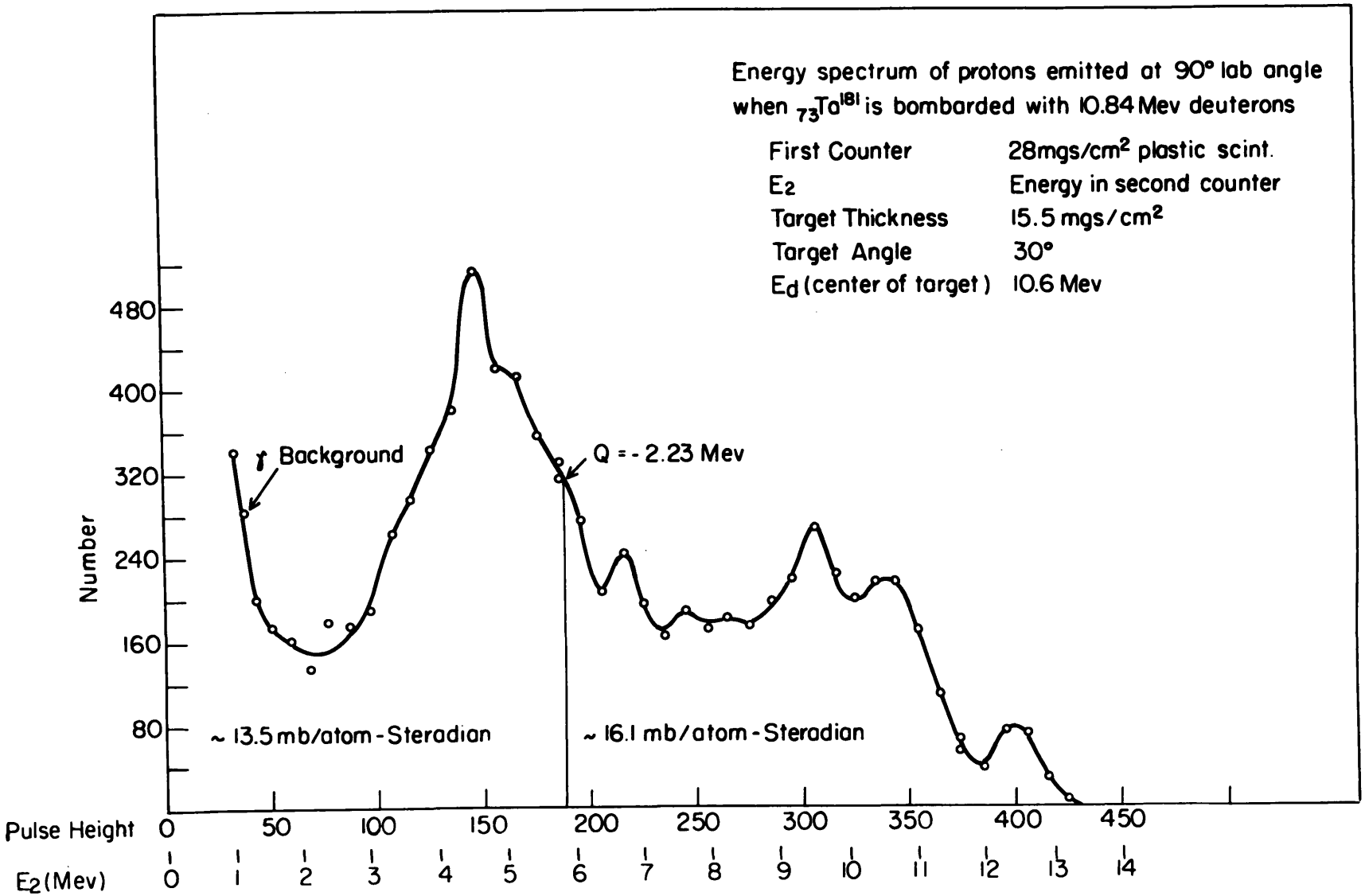
Energy spectrum of protons emitted at 90° lab angle
when $_{73}Ta^{181}$ is bombarded with 10.84 Mev deuterons
First Counter 28mgs/cm² plastic scint.
E2 Energy in second counter
Target Thickness 15.5 mgs/cm²
Target Angle 30°
Ed (center of target) 10.6 Mev
Number
480
400
320
240
160
80
Background
Q = - 2.23 Mev
~ 13.5 mb/atom - Steradian
~ 16.1 mb/atom - Steradian
Pulse Height 0 50 100 150 200 250 300 350 400 450
E2 (Mev) 0 1 2 3 4 5 6 7 8 9 10 11 12 13 14

Figure 26

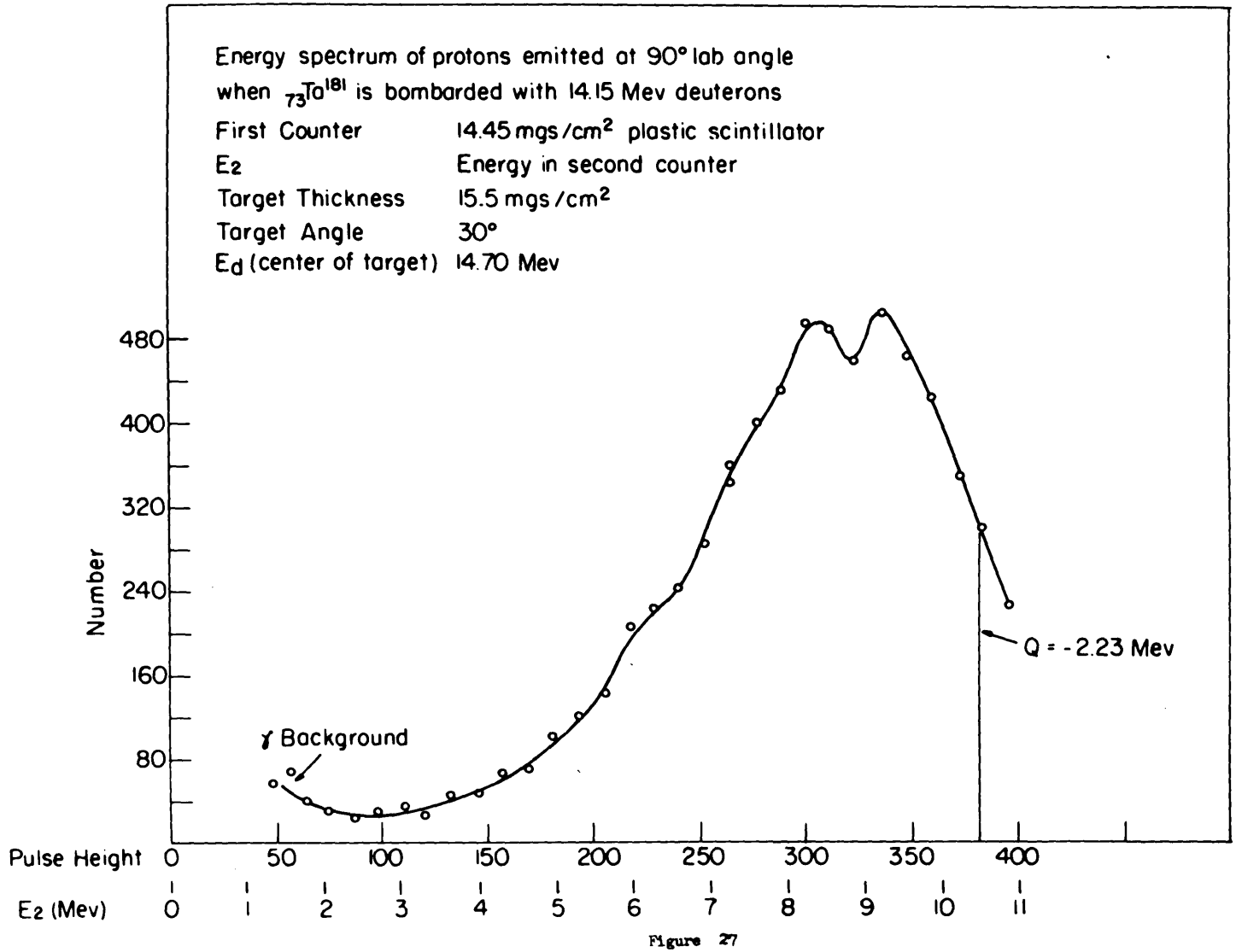
Energy spectrum of protons emitted at 90° lab angle
when $_{73}Ta^{181}$ is bombarded with 14.15 Mev deuterons
First Counter 14.45 mgs/cm² plastic scintillator
E2 Energy in second counter
Target Thickness 15.5 mgs/cm²
Target Angle 30°
Ed (center of target) 14.70 Mev
Number
480
400
320
240
160
80
γ Background
Q = -2.23 Mev
Pulse Height 0 50 100 150 200 250 300 350 400
E2 (Mev) 0 1 2 3 4 5 6 7 8 9 10 11

Figure 27

The energy of the direct deuteron beam was reduced by inserting aluminum foils with the foil changer. This increased the γ-ray background seriously. To check this background, the proton spectra were repeated using the 14.45 mgs/cm^2 plastic scintillator in the first counter. Figure 27 shows one of the spectra that was repeated.

The total cross sections were estimated by graphically integrating the angular distributions. The values obtained are as follows:

TABLE 2

Summary of $Ta^{181}(d,p)Ta^{182}$ Cross Sections

E_d	E_d (Center of Target)	$\sigma_<$	$\sigma_>$
14.75	14.55	240	103
13.97	13.76	299	140
12.80	12.57	276	216
11.71	11.50	228	283
10.84	10.60	183	230

where:

E_d = the deuteron beam energy.

$\sigma_<$ = the cross section for $Q < -2.23$ Mev.

$\sigma_>$ = the cross section for $Q > -2.23$ Mev.

$_{82}Pb^{206}$ (24.1 mgs/cm^2 metal foil)

Figure 28 shows the proton energy spectrum observed in the second counter at 75 degrees. The spectrum was also observed at 50, 60, 90, 120, and 150 degrees. The angular distributions have the same shapes as those for Pb^{207} (see Figure 30). The total cross sections were estimated to be 227 millibarns/atom for $Q < -2.23$ Mev and 131 millibarns/atom for $Q > -2.23$ Mev.

$_{82}Pb^{207}$ (23 mgs/cm^2 metal foil)

The proton energy spectrum observed in the second counter at an angle of 75 degrees is shown in Figure 29. The spectrum was also observed at 50, 60, 90, 120, and 150 degrees. Figure 30 shows the angular distributions obtained. The total cross sections were estimated to be 250 millibarns/atom for $Q < -2.23$ Mev and 146 millibarns/atom for $Q > -2.23$ Mev.

$_{82}Pb^{208}$ (21.2 mgs/cm^2 metal foil)

The proton energy spectrum was observed at counter angles of 50, 60, 75, 90, 120, and 150 degrees. Figure 31 shows the spectrum observed at 75 degrees. The angular distributions were the same as that for Pb^{207}. The cross sections were estimated to be 230 millibarns/atom for $Q < -2.23$ Mev and 133 millibarns/atom for $Q > -2.23$ Mev.

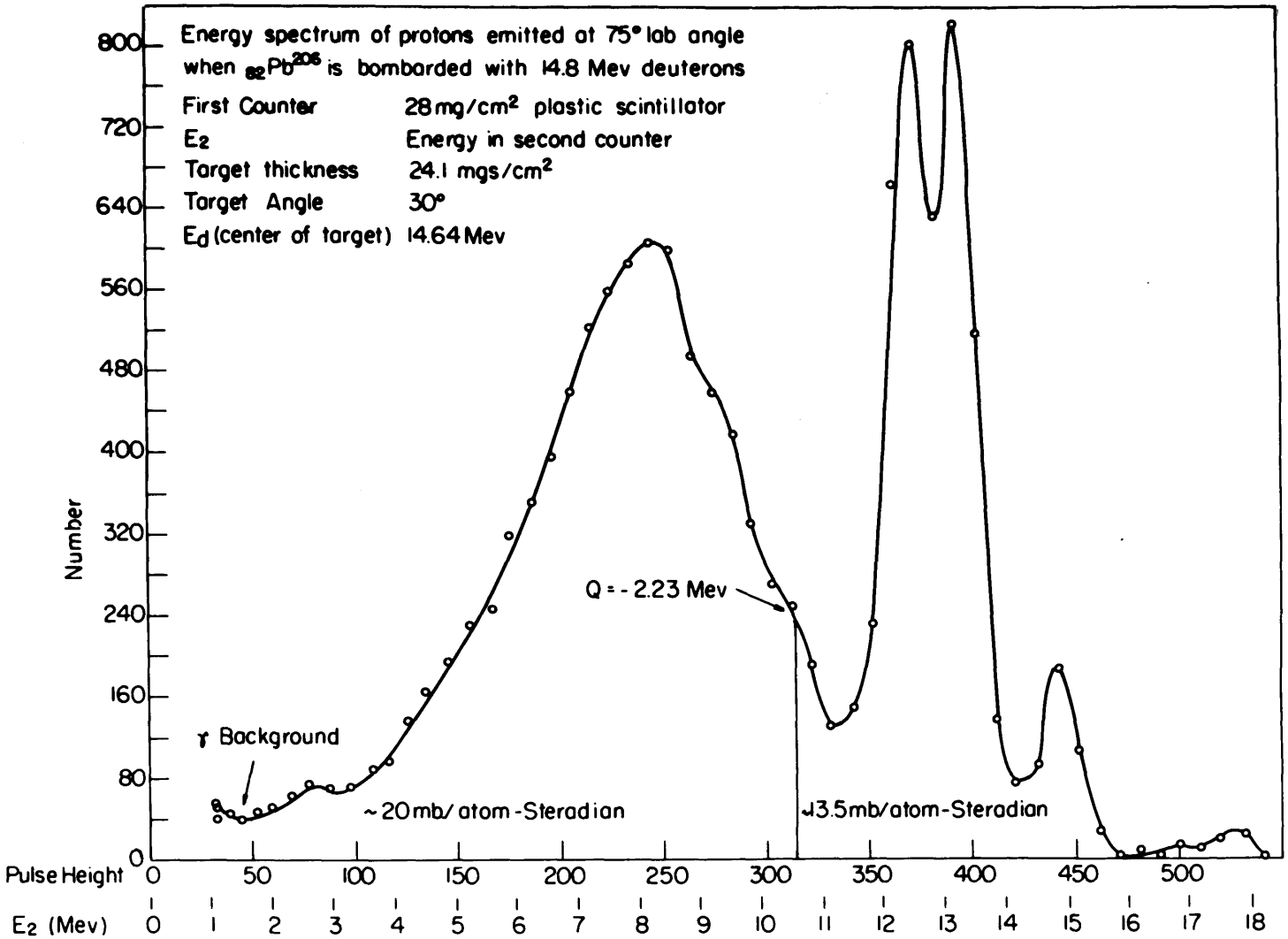
Energy spectrum of protons emitted at 75° lab angle
when $_{82}Pb^{206}$ is bombarded with 14.8 Mev deuterons
First Counter 28 mg/cm² plastic scintillator
E2 Energy in second counter
Target thickness 24.1 mgs/cm²
Target Angle 30°
Ed (center of target) 14.64 Mev
Number
Pulse Height
E2 (Mev)
Q = - 2.23 Mev
γ Background
~20 mb/ atom - Steradian
~3.5 mb/atom-Steradian

Figure 28

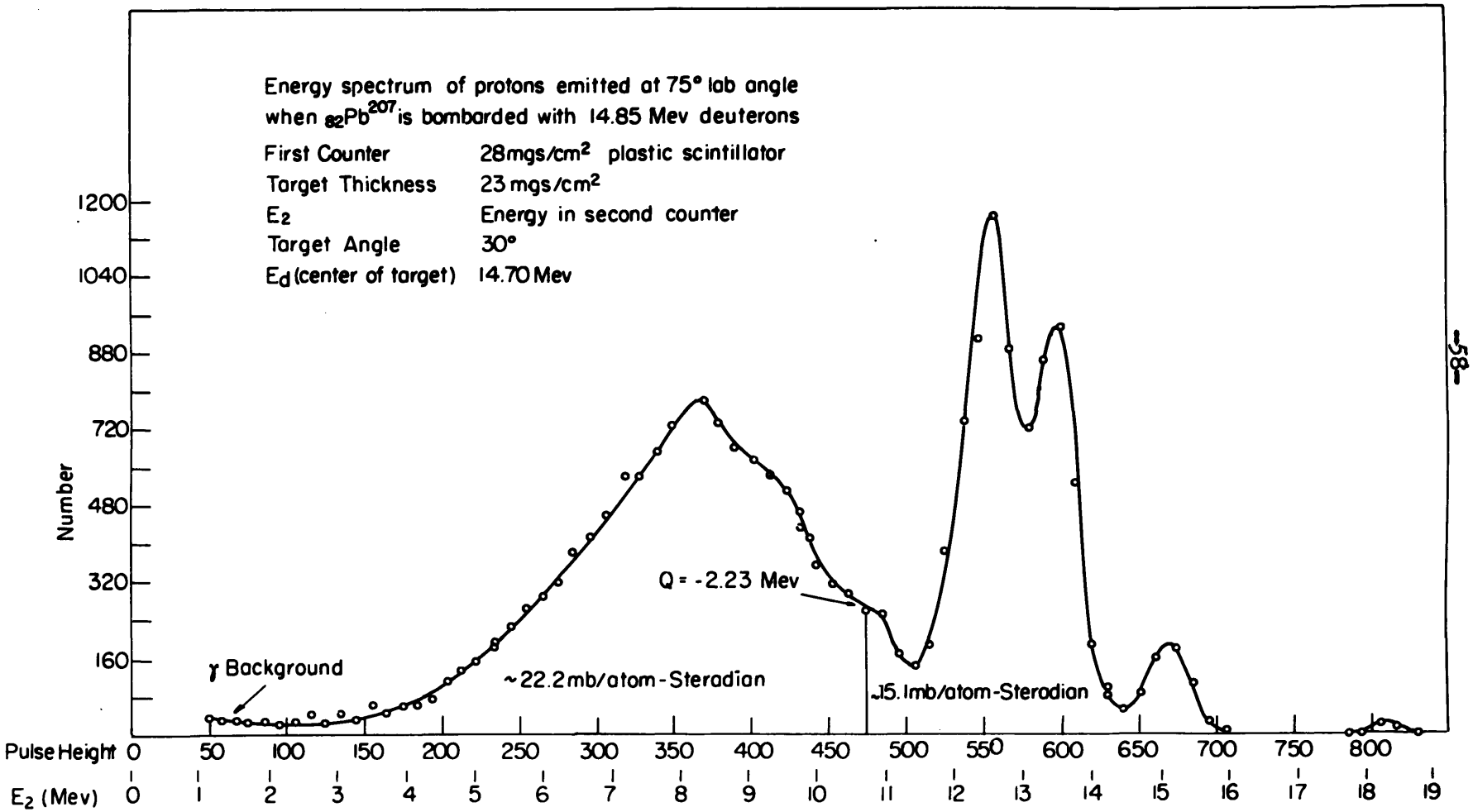
Energy spectrum of protons emitted at 75° lab angle
when $_{82}Pb^{207}$ is bombarded with 14.85 Mev deuterons
First Counter 28mgs/cm² plastic scintillator
Target Thickness 23 mgs/cm²
E_2 Energy in second counter
Target Angle 30°
E_d (center of target) 14.70 Mev
Number
1200
1040
880
720
480
320
160
γ Background
~22.2mb/atom-Sterodian
Q = -2.23 Mev
~15.1mb/atom-Sterodian
Pulse Height 0 50 100 150 200 250 300 350 400 450 500 550 600 650 700 750 800
E_2 (Mev) 0 1 2 3 4 5 6 7 8 9 10 11 12 13 14 15 16 17 18 19

Figure 29

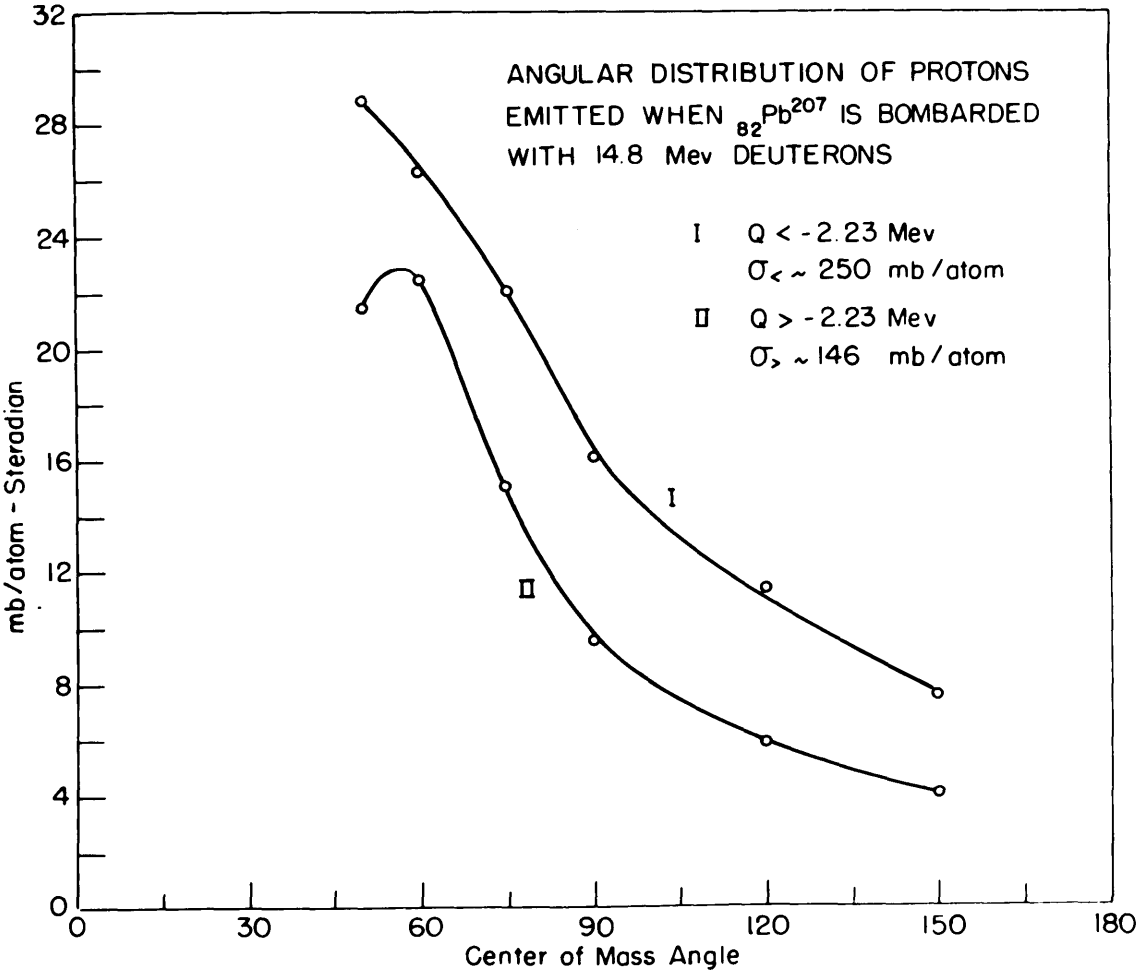
ANGULAR DISTRIBUTION OF PROTONS
EMITTED WHEN $_{82}Pb^{207}$ IS BOMBARDED
WITH 14.8 Mev DEUTERONS
I Q < -2.23 Mev
$\sigma_<$ ~ 250 mb/atom
II Q > -2.23 Mev
$\sigma_>$ ~ 146 mb/atom
I
II
mb/atom - Steradian
Center of Mass Angle
0
4
8
12
16
20
24
28
32
0
30
60
90
120
150
180

Figure 30

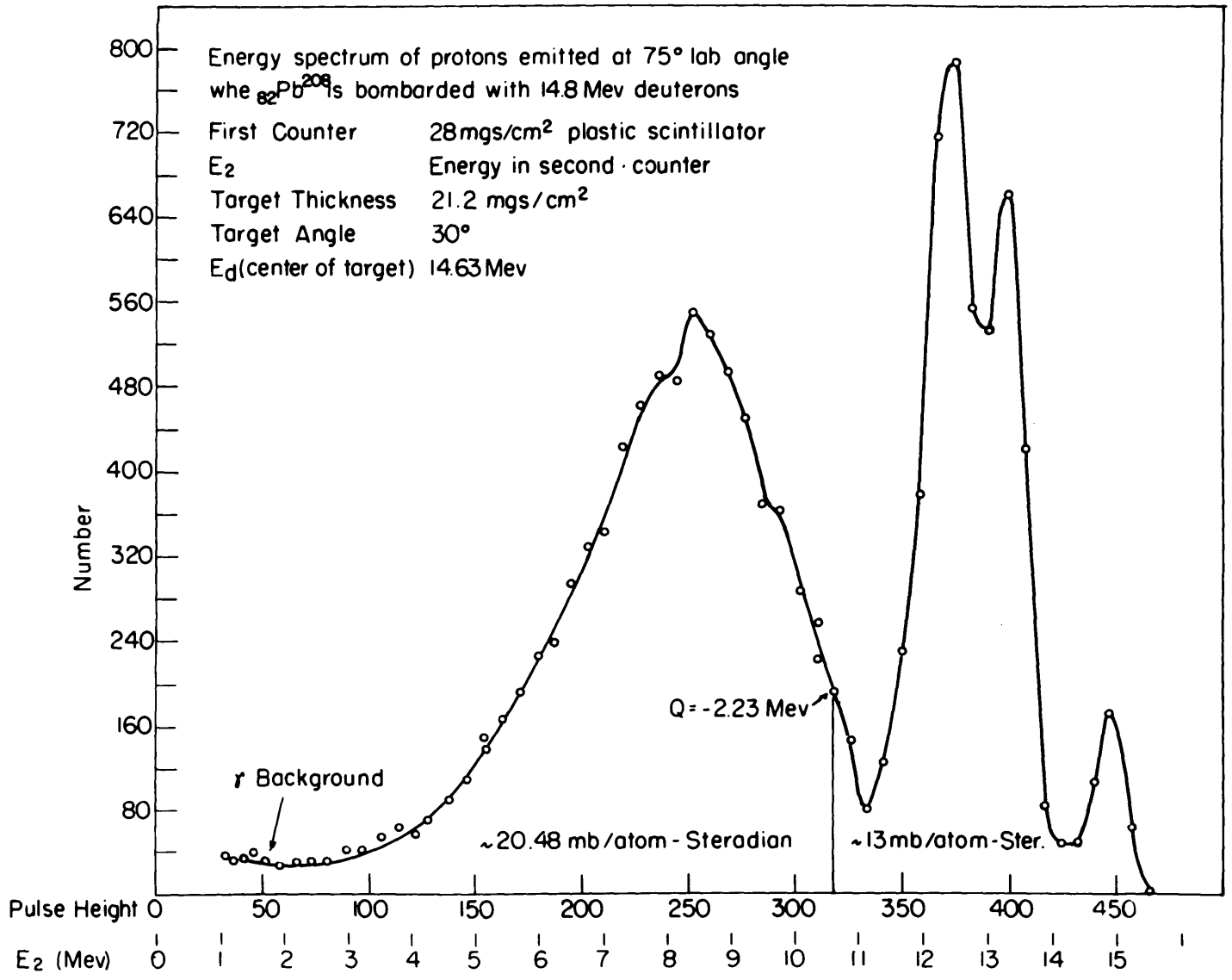
Energy spectrum of protons emitted at 75° lab angle
whe $_{82}Pb^{208}$ is bombarded with 14.8 Mev deuterons
First Counter 28 mgs/cm² plastic scintillator
E2 Energy in second counter
Target Thickness 21.2 mgs/cm²
Target Angle 30°
Ed(center of target) 14.63 Mev
Number
800
720
640
560
480
400
320
240
160
80
Q = -2.23 Mev
γ Background
~20.48 mb/atom - Steradian
~13 mb/atom-Ster.
Pulse Height 0 50 100 150 200 250 300 350 400 450
E2 (Mev) 0 1 2 3 4 5 6 7 8 9 10 11 12 13 14 15

Figure 31

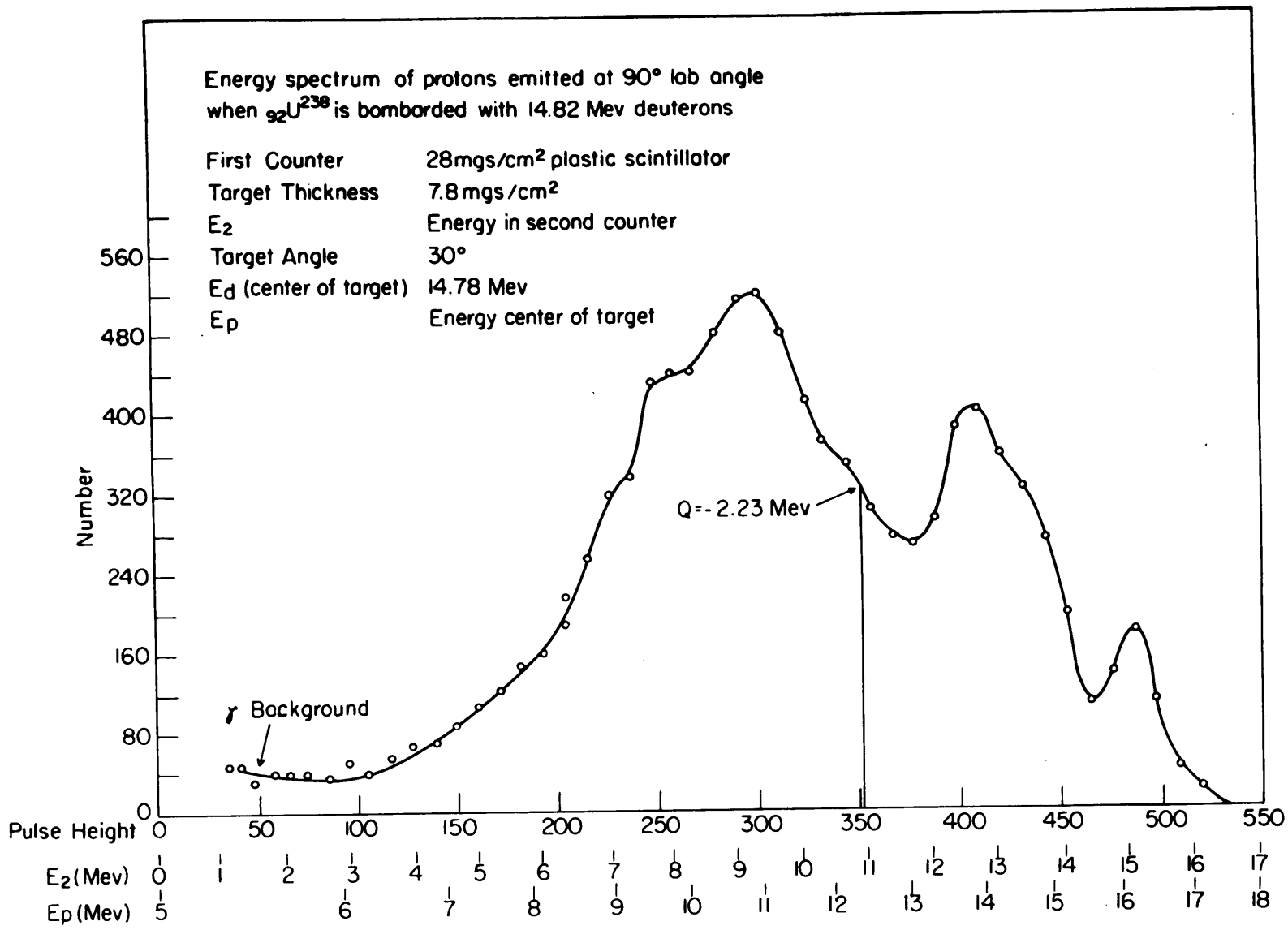
Energy spectrum of protons emitted at 90° lab angle
when $_{92}U^{238}$ is bombarded with 14.82 Mev deuterons
First Counter 28mgs/cm² plastic scintillator
Target Thickness 7.8mgs/cm²
E2 Energy in second counter
Target Angle 30°
Ed (center of target) 14.78 Mev
Ep Energy center of target
Number
Q=-2.23 Mev
γ Background
Pulse Height
E2(Mev)
Ep(Mev)

Figure 32

$_{92}U^{238}$ (7.8 mgs/cm^2 metal foil)

Figure 32 shows the proton energy spectrum observed in the second counter at an angle of 90 degrees. The energy spectrum was also observed at 60, 120, and 150 degrees. No cross-section measurements were obtained in this case.

V. INTERPRETATION OF DATA

The data for each case were calculated to determine the energy spectrum of the protons emitted from the center of the target. In addition, the center-of-mass corrections were applied, because theoretical calculations are usually made in center-of-mass coordinates. However, since all of the targets studied were relatively heavy, the center-of-mass corrections were almost negligible.

For convenience in the calculations, curves were prepared showing the energies of the protons (E_p) emitted from the center of the target (with the center-of-mass corrections applied) as a function of E_2 for each target and each angle. Figure 17 shows one example.

Energy spectra are usually represented in the form dN/dE as a function of energy, where dN is the number of particles in the infinitesimal energy interval dE. Experimentally, to obtain reasonable counting rates, the energy intervals are far from infinitesimal; therefore, the expression dN/dE is more appropriately written as $\Delta N/\Delta E$ where ΔN is the number of particles in the finite but constant energy interval ΔE. In the cases where dN/dE varies only a small amount in the energy interval ΔE, the spectrum shape obtained by plotting $\Delta N/\Delta E$ as a function of E is almost identical to the true spectrum shape.

In analyzing the data for these experiments, it was assumed that the NaI(Tl) crystal had a linear response to the particle energy

loss in the crystal. Since the window width of the analyzer was constant during an experiment, no ΔE correction was applied to the data in presenting the E_2 spectra.

In examining Figure 17, it is observed that $\Delta E_p/\Delta E_2$ is not a constant. Therefore, in order to obtain a reasonably correct E_p energy spectrum, i.e., $\Delta N/\Delta E_p$, as a function of E_p where ΔN is the number of protons in the finite but constant energy interval ΔE_p, the number of particles observed at each energy E_p was multiplied by the factor F where $F = \Delta E_p/\Delta E_2$. For convenience in applying this correction factor (F), curves were prepared showing F as a function of E_2 for each case. Figure 33 shows one example. Figure 34 shows the corrected E_p spectrum for the protons emitted from $_{82}Pb^{208}$ at 75 degrees from the incident deuteron beam. In applying the corrections, the γ-proton coincidence background is distorted.

The center-of-mass angle for the protons observed at a given laboratory angle depends upon the proton energy. However, for all the targets observed in these experiments, the center-of-mass angles differ at most 1-1/2 degrees from the laboratory angles. Since the energy spectra changed a negligible amount over this angle interval, it was not deemed necessary to give the center-of-mass angle for each proton energy.

The proton energy spectra were divided into two parts, using $Q = -2.23$ Mev as the dividing line. This division is made because

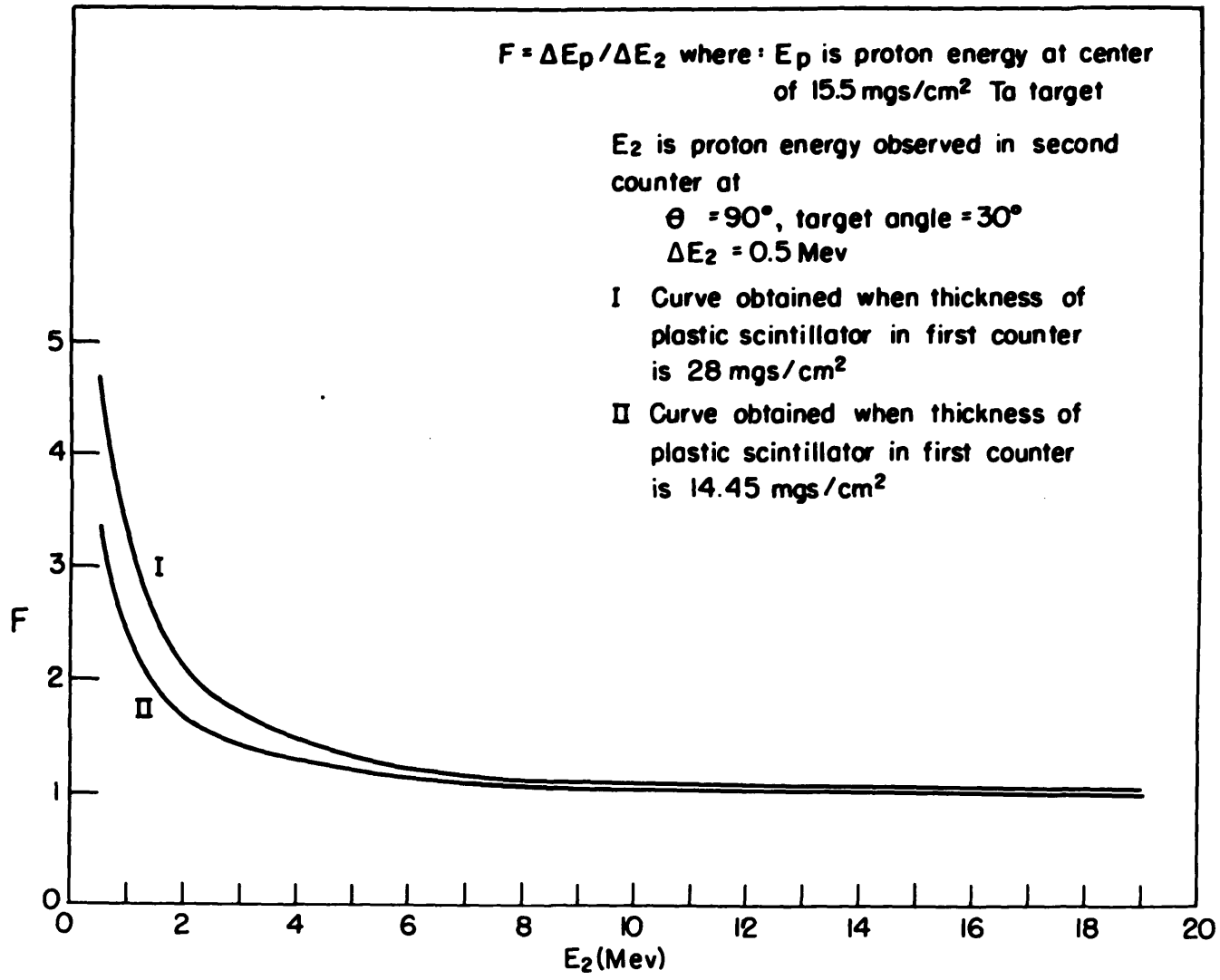
F = ΔEp/ΔE2 where: Ep is proton energy at center of 15.5 mgs/cm² Ta target
E2 is proton energy observed in second counter at
θ = 90°, target angle = 30°
ΔE2 = 0.5 Mev
I Curve obtained when thickness of plastic scintillator in first counter is 28 mgs/cm²
II Curve obtained when thickness of plastic scintillator in first counter is 14.45 mgs/cm²
F
E2(Mev)
0
1
2
3
4
5
0
2
4
6
8
10
12
14
16
18
20
I
II

Figure 33

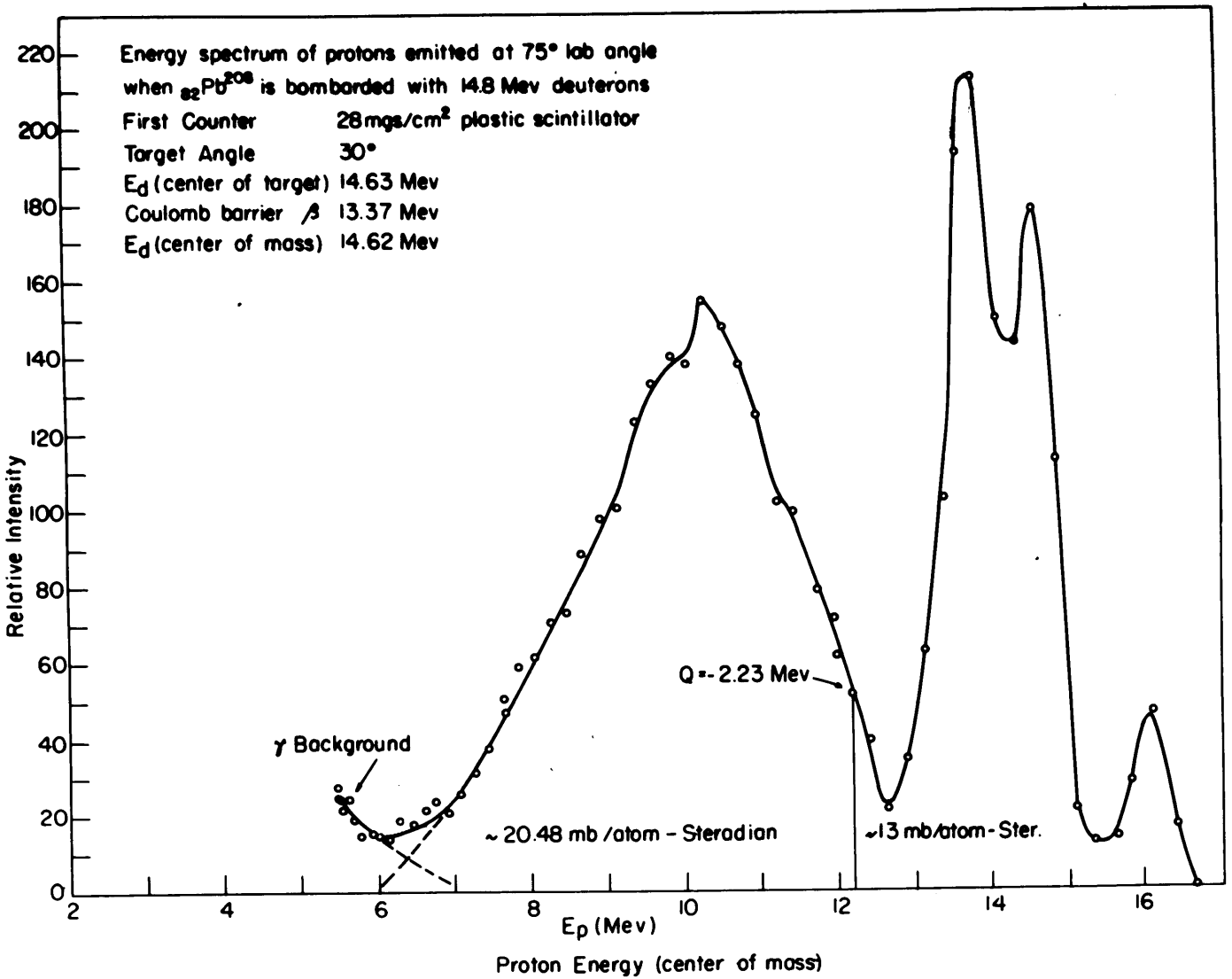
Energy spectrum of protons emitted at 75° lab angle
when $_{82}Pb^{208}$ is bombarded with 14.8 Mev deuterons
First Counter 28 mgs/cm² plastic scintillator
Target Angle 30°
E_d (center of target) 14.63 Mev
Coulomb barrier β 13.37 Mev
E_d (center of mass) 14.62 Mev
Relative Intensity
Q = - 2.23 Mev
γ Background
~ 20.48 mb /atom - Steradian
~13 mb/atom - Ster.
E_p (Mev)
Proton Energy (center of mass)

Figure 34

the protons from (d,p) reactions with $Q > -2.23$ Mev leave the residual nucleus in states in which the neutron is bound. The protons for which $Q < -2.23$ Mev leave the residual nucleus in unbound states, making it possible for the residual nucleus to decay by neutron emission. Proton spectra from (d,p) reactions with $Q > -2.23$ Mev have been studied previously (G1) and are included here only for a comparison with the proton spectra for $Q < -2.23$ Mev.

In considering the proton spectra with $Q < -2.23$ Mev, a broad peak is observed in each case. Superposed on this broad peak is a variation of proton intensity indicating a variation of level density in the residual nucleus, especially between the broad peak and line for $Q = -2.23$ Mev. For experimental reasons the spectra were not investigated in sufficient detail to establish the exact energy-level structure.

The low-energy parts of the proton spectra show what appears to be a coulomb barrier effect. It is believed that, if the γ-proton coincidence background was absent, an experimental cutoff would be observed, where "experimental cutoff" is construed to mean that the intensity decreases to a very small fraction of the intensity that could be observed with the experimental setup. The data curves were extrapolated to zero intensity in order to obtain an estimate of where the experimental cutoff would be. Although it was not definitely established that an experimental cutoff exists, a study of the extrapolated points is justified because it offers a method for

studying the slope and position of the coulomb barrier effect. This study has helped in understanding what types of reactions are responsible for the low-energy parts of the proton spectra.

In analyzing the data in the manner described, the following points are noted:

1. Protons are observed several Mev below the coulomb barrier for protons, indicating that the barrier effect differs from the ordinary coulomb barrier penetration of protons emerging from a compound nucleus;

2. The extrapolated cutoff energy (E_c) and the shape of the low-energy part of the spectrum seem to be independent of angle within the accuracy of the experiments;

3. Data on the Pb isotopes shows that, within the accuracy of the experiment, the extrapolated cutoff energy is independent of neighboring isotopes which indicates that it depends only on the coulomb barrier.

4. The extrapolated cutoff energy varies slowly as a function of deuteron bombarding energy. Figure 35 shows a summary of the low-energy parts of the spectra for $_{73}Ta^{181}$ with deuteron bombarding energies ranging from 10.84 to 14.75 Mev. The extrapolated energy over this range varies less than 500 kev.

5. The extrapolated cutoff energy increases with increasing barrier height. Figure 36 shows a summary of the low-energy parts of the spectra for all targets studied.

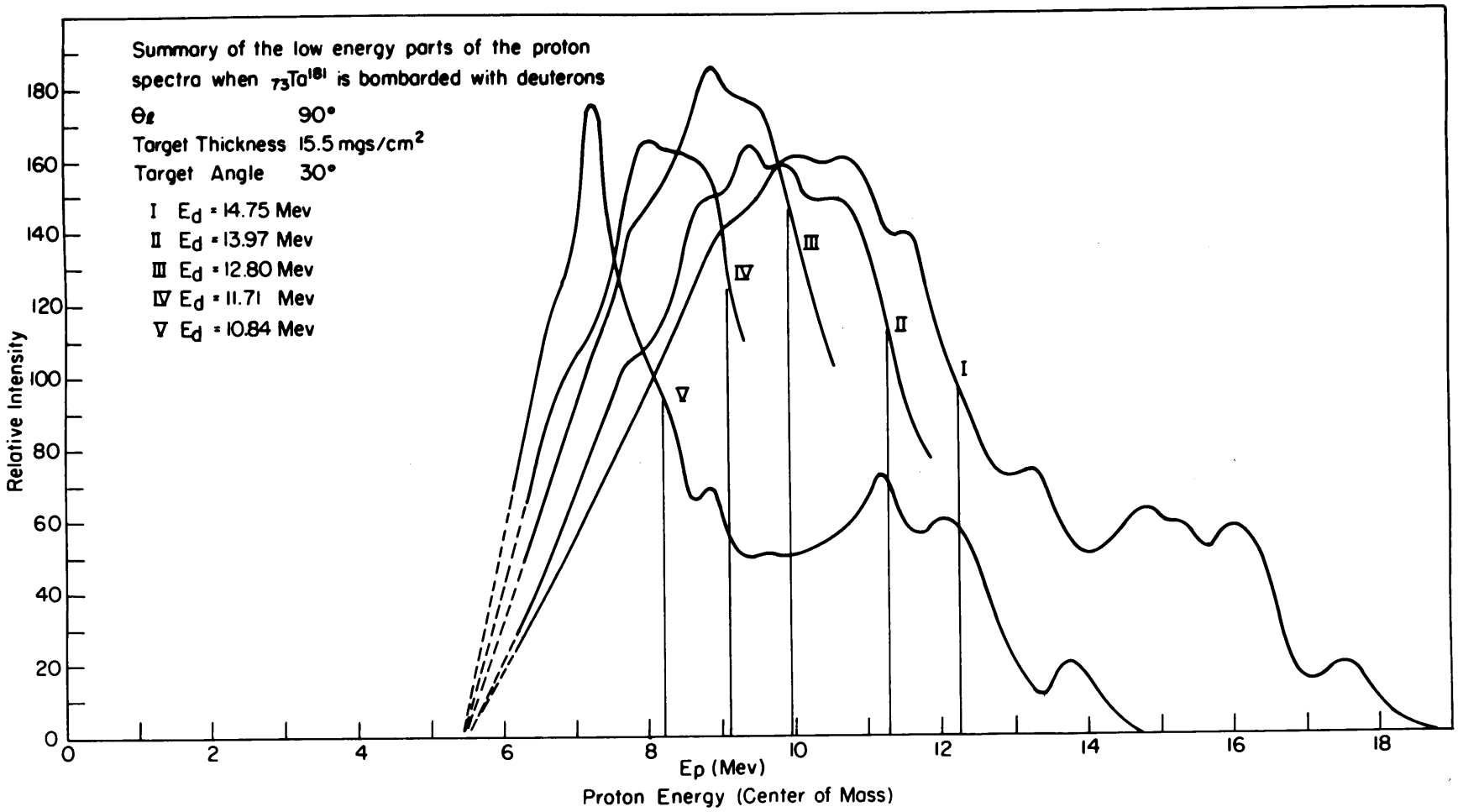
Summary of the low energy parts of the proton spectra when $_{73}Ta^{181}$ is bombarded with deuterons
θ_ℓ 90°
Target Thickness 15.5 mgs/cm²
Target Angle 30°
I E_d = 14.75 Mev
II E_d = 13.97 Mev
III E_d = 12.80 Mev
IV E_d = 11.71 Mev
V E_d = 10.84 Mev
Relative Intensity
0
20
40
60
80
100
120
140
160
180
0
2
4
6
8
10
12
14
16
18
Ep (Mev)
Proton Energy (Center of Mass)

Figure 35

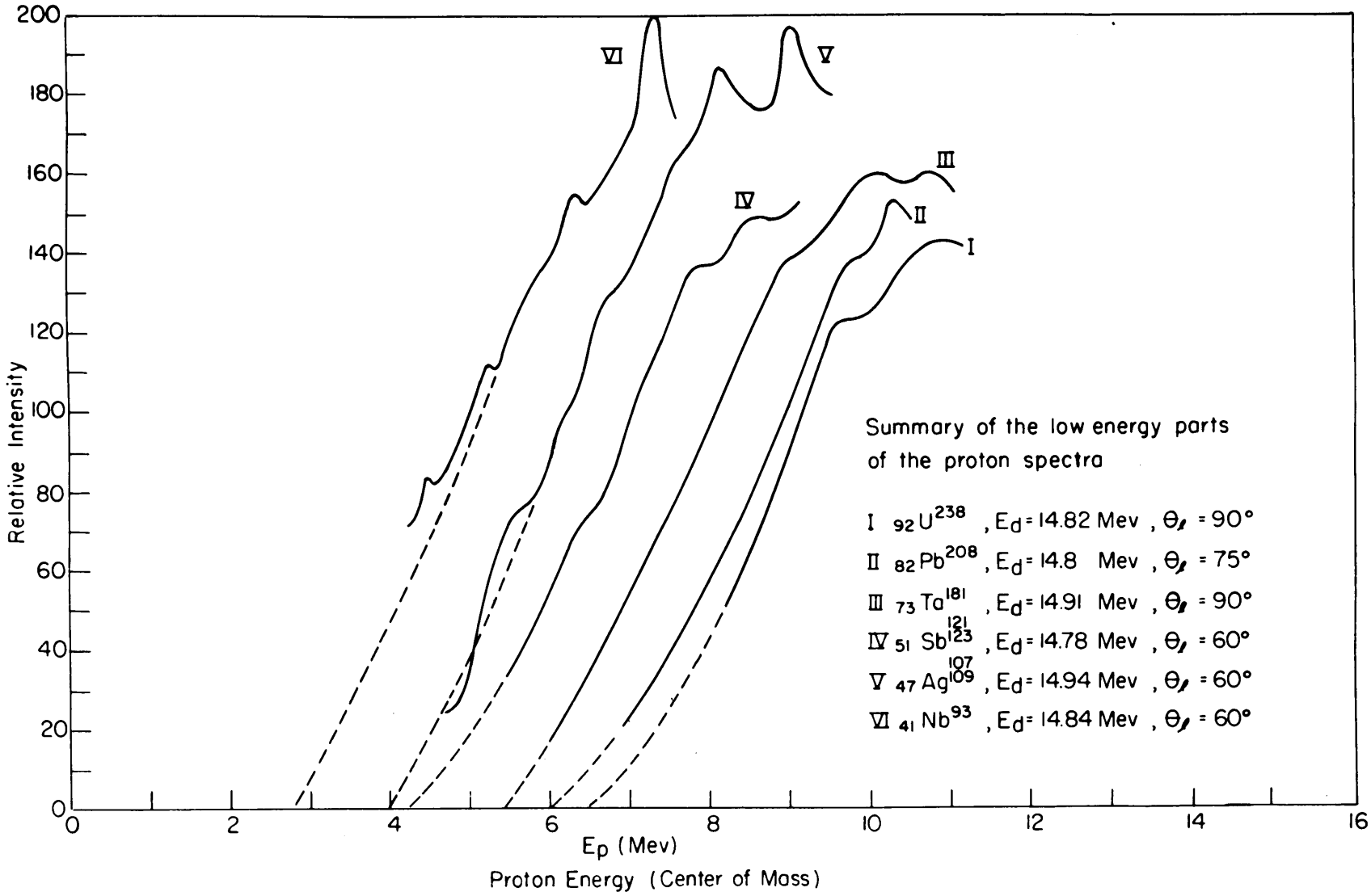
Relative Intensity
Ep (Mev)
Proton Energy (Center of Mass)
Summary of the low energy parts of the proton spectra
I 92U238 , Ed = 14.82 Mev , θl = 90°
II 82Pb208 , Ed = 14.8 Mev , θl = 75°
III 73Ta181 , Ed = 14.91 Mev , θl = 90°
IV 51Sb121,123 , Ed = 14.78 Mev , θl = 60°
V 47Ag107,109 , Ed = 14.94 Mev , θl = 60°
VI 41Nb93 , Ed = 14.84 Mev , θl = 60°

Figure 36

All of the points noted above appear to be qualitatively consistent with a stripping model in which the deuteron is first polarized and stretched by the coulomb field, and then the neutron is stripped off leaving the proton outside the coulomb barrier. This interpretation is supported by a comparison of the angular distributions and estimated cross sections for the protons with $Q < -2.23$ Mev with the angular distributions and estimated cross sections for the protons with $Q > -2.23$ Mev. Agreement between Butler's (d,p) stripping theory (B1) and experimental results (B2) for protons with $Q > -2.23$ Mev indicates that these protons definitely result from (d,p) stripping. Figures 20 and 30 show a comparison of the angular distributions. Table 3 shows a comparison of the estimated cross sections.

TABLE 3

Summary of Estimated Cross Sections
and Extrapolated Cutoff Energies

Target	E_d Mev	E_d (c.m.) Mev	B Mev	$\sigma_<$ mb	$\sigma_>$ mb	σ_T mb	E_c Mev
$_{92}U^{238}$	14.82	14.53	14.25				6.6
$_{82}Pb^{208}$	14.8	14.35	13.37	230	133	363	6.35
$_{82}Pb^{207}$	14.85	14.42	13.37	250	146	396	6.48
$_{82}Pb^{206}$	14.80	14.36	13.37	227	131	358	6.40
$_{73}Ta^{181}$	14.75	14.24	12.38	240	103	343	5.80
$_{73}Ta^{181}$	13.97	13.47	12.38	299	140	439	5.80
$_{73}Ta^{181}$	12.80	12.32	12.38	276	216	492	5.70
$_{73}Ta^{181}$	11.71	11.25	12.38	228	283	511	5.60
$_{73}Ta^{181}$	10.84	10.35	12.38	183	230	413	5.50
$_{51}Sb^{121}{}^{123}$	14.78	14.23	9.87	277	128	405	4.33
$_{47}Ag^{107}{}^{109}$	14.94	14.30	9.48	284	100	384	4.20
$_{41}Nb^{93}$	14.89	13.85	8.69				3.50

where: E_d = deuteron beam energy in laboratory coordinates.

$E_d(c.m.)$ = deuteron beam energy in center-of-mass coordinates.

B = the coulomb barrier height.

$\sigma_<$ = the estimated cross section for $Q < -2.23$.

$\sigma_>$ = the estimated cross section for $Q > -2.23$.

σ_T = the total cross section.

E_c = the extrapolated cutoff energy.

Table 3 also shows a summary of the extrapolated cutoff energies. The nearest distance of approach between the protons, at the extrapolated cutoff energy, and the nuclear surface for $_{73}Ta^{181}$, assuming that the protons stayed outside the coulomb barrier, was calculated from the formula:

$$E_c = \frac{Z\, z\, e^2}{R + X}, \qquad R = 1.5A^{1/3} \times 10^{-13} \text{ cm},$$

where:

Z = the charge of the nucleus.

z = the proton charge.

e = the charge on an electron.

R = the calculated nuclear radius.

A = the nuclear mass number.

X = the calculated nearest distance of approach.

X was calculated to be 9.634×10^{-13} cm. Assuming that the low-energy protons are from (d,p) stripping reactions, X can be considered as the extent of the polarized deuteron wave function. Figure 37 shows a curve of E_c as a function of Z calculated from the above formula, using $X = 9.634 \times 10^{-13}$ cm. The other experimental values of E_c show good agreement with the calculated curve. A better agreement could not be expected, because of the precision of the experiments and the variation of actual nuclear radii from the formula $R = 1.5\ A^{1/3} \times 10^{-13}$ cm.

At first, it would seem that the calculated distance of approach (X) is much greater than would be expected from the extent of the deuteron wave function obtained from other considerations. However, theoretical (d,p) excitation functions, which show fair agreement with experimental excitation functions (P1), indicate the (d,p) reactions can occur when the protons are a distance X from the nuclear surface. These excitation functions show the same kind of barrier effect as observed in the proton spectra. The extrapolated threshold energies for the excitation functions show agreement with the calculated E_c values (see Figure 37). Because of the energy resolution obtained with the stacked-foil method for obtaining excitation functions (C1), the agreement is as good as could be expected.

It is believed that a slight variation of Peaslee's semiclassical theory (P1) for calculating (d,p) excitation functions can be used to explain the low-energy parts of the proton spectra observed

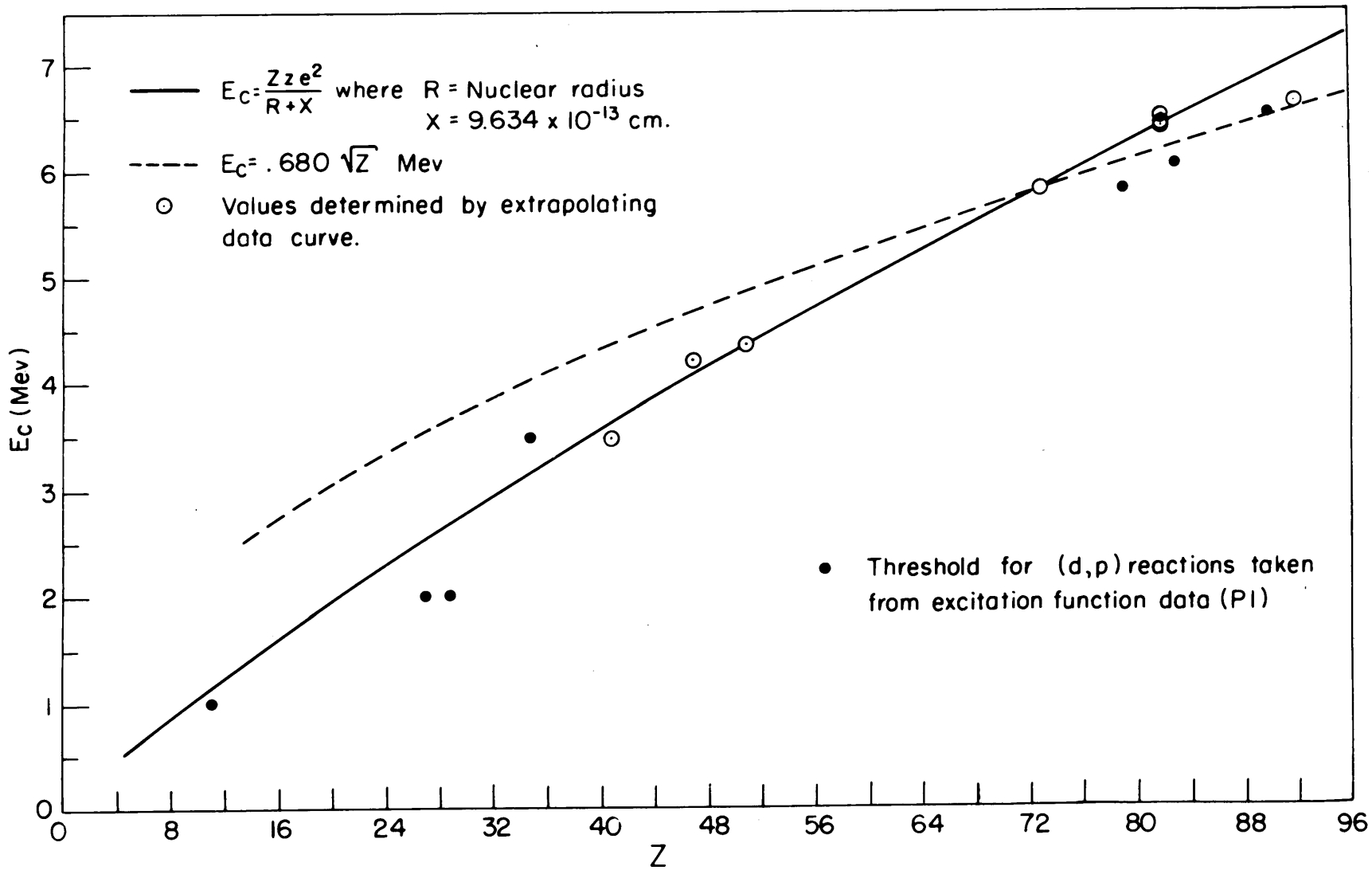
$E_C = \frac{Zze^2}{R+X}$ where R = Nuclear radius
X = 9.634 x 10^{-13} cm.
$E_C = .680\sqrt{Z}$ Mev
Values determined by extrapolating data curve.
Threshold for (d,p) reactions taken from excitation function data (P1)
Ec (Mev)
Z
0
1
2
3
4
5
6
7
8
16
24
32
40
48
56
64
72
80
88
96

Figure 37

in the present experiments. An attempt will be made in the very near future to use a variation of Peaslee's theory for calculating these proton spectra.

Recently, exact wave-mechanical calculations for (d,p) stripping reactions, which include coulomb effects, were made by Tobocman (T2). If the low-energy protons in the present experiments are due to stripping reactions, it would seem that Tobocman's theory should show a proton energy dependence for the cross section that is in agreement with the experiments. However, the proton energies appear in the theory in such a complicated way that it is almost impossible to check the theory with the experiments. Tobocman's theory is better suited for single proton energy levels.

The possibility exists that some of the low-energy protons are due to electric breakup of the deuterons. Qualitative arguments can be used to show that at least the extreme low-energy parts of the spectra are not due to electric breakup processes. One crude argument that can be used is the following:

For a given deuteron energy, the electric field required to break up the deuteron is given by F_e. At the point where this electric field is reached, the deuteron can be broken up, leaving a proton just outside the coulomb barrier at zero kinetic energy. The proton would then gain a kinetic energy while sliding down the barrier equal to the potential energy at the point of breakup. This

would be the minimum energy of protons observed that were due to the electric breakup process. If it is assumed that at the breakup point the kinetic energy of the deuteron is only slightly different from the incident deuteron energy, then for a given incident deuteron energy, the electric field at the breakup point is approximately the same for all nuclei. The electric field is given by

$$F_e = \frac{Z\,e}{r^2}$$

where r is the distance from the center of the nucleus at breakup. The corresponding coulomb potential is given by

$$V_e = \frac{Z\,e}{r} = \sqrt{F_e\,Z\,e}\,.$$

The potential energy of the proton at r is

$$E_p = z\,e\,\sqrt{F_e\,Z\,e} = K\sqrt{Z}\,.$$

This would predict that, if E_c were determined by the electric breakup process, then for a given deuteron beam energy $E_c = K\sqrt{Z}$. Figure 37 shows this curve with K determined from the $_{73}Ta^{181}$ data. The experimental data do not fit this curve very well.

It would seem that electric breakup processes could only compete favorably with stripping reactions when the electric field is strong enough to break up the deuteron before the deuteron comes close enough for a stripping reaction.

Calculations by Guth and Mullin (G3) predict cross sections of approximately 200 millibarns caused by electric breakup processes for targets of $Z > 29$ bombarded with 15-Mev deuterons. Since the calculations do not show the proton energy spectra, no direct comparison with the experimental data could be made. However, it is expected that the cross sections predicted by Guth and Mullin are much too high.

VI. SUMMARY

A particle-selection technique is described which makes it possible to identify readily the reaction particles from deuteron-induced reactions. The particles are detected with a counter combination which consists of two scintillation counters mounted on one movable arm in the scattering chamber. The first is a thin plastic scintillation counter which measures dE/dx of the reaction particles, and the second is a NaI(Tl) scintillation counter which measures the remaining energy of the reaction particles after they pass through the thin counter. Appropriate electronic apparatus is used in conjunction with the counter combination which makes it possible to obtain the energy spectra of the emitted particles.

Because of the nonlinear response of the plastic scintillator to particles of high dE/dx, tritons below 15 Mev are not well separated from deuterons. This separation can be improved by replacing the thin plastic scintillation counter with a linear counter that has the same resolution. A thin gas proportional counter which has a resolution of approximately 15 percent would be a good substitute.

Because of experimental difficulties, the protons with energies corresponding to (d,p) reactions with $Q < -2.23$ Mev had not in the past been observed. However, the recent development of a convenient particle-selection technique has made it possible to study the entire proton spectra from targets with $Z > 41$. It was decided to conduct a study of the low-energy protons from selected targets bombarded with the M.I.T. Cyclotron deuteron beam which would determine

what processes are most important in producing the low-energy protons. In this study, the proton spectra from niobium, silver, antimony, tantalum, three lead isotopes, and uranium bombarded with the direct deuteron beam were observed at several angles. In addition, the proton energy spectrum from tantalum was observed at several deuteron beam energies ranging from approximately 10.5 to 15 Mev. In these measurements the direct deuteron beam energy was reduced by inserting aluminum foils.

The properties of the proton spectra with $Q < -2.23$ Mev can be summarized as follows:

1. In each case a broad peak was observed.

2. Superposed on the broad peak is a variation of proton intensity, especially between the peak and the line at $Q = -2.23$ Mev, which indicates a variation of the density of energy levels in the residual nucleus.

3. The angular distribution for all the protons with $Q < -2.23$ Mev in each case is peaked forward, and the shape of this angular distribution is very similar to that for $Q > -2.23$ Mev.

4. The total cross sections for $Q < -2.23$ Mev are of the same order of magnitude as for $Q > -2.23$ Mev.

5. The low-energy part of each proton spectrum shows what appears to be a coulomb barrier effect. However, protons are observed several Mev below the coulomb barrier for protons, indicating that the barrier effect differs from the ordinary coulomb barrier penetration of protons emerging from a compound nucleus.

6. An apparent experimental cutoff (E_c) is observed at the low-energy end of the spectrum which has the following properties:

a. E_c is independent of angle within the accuracy of the experiments.

b. E_c is the same for neighboring isotopes within the accuracy of the experiments.

c. E_c varies less than 500 kev for deuteron bombarding energies ranging from 10.84 to 14.75 Mev.

d. E_c increases with increasing barrier height at a rate that indicates it is equal to the potential energy of the proton at a distance of approximately 9.6×10^{-13} cm from the nuclear surface.

e. E_c is approximately the same as the apparent deuteron threshold energy for (d,p) reactions.

All the points noted above appear to be qualitatively consistent with a stripping model in which the deuteron is first polarized and stretched by the coulomb field, and then the neutron is stripped off leaving the proton outside the coulomb barrier. Electric breakup of the deuterons appears to contribute very little to the proton spectra.

It is believed that a slight variation of Peaslee's semiclassical theory (P1) for calculating (d,p) excitation functions can be used to explain the low-energy parts of the proton spectra. An attempt will be made in the very near future to use a variation of Peaslee's theory for calculating these proton spectra.

BIBLIOGRAPHY

A1 F. A. Aschenbrenner, M.I.T. Laboratory for Nuclear Science, Progress Report (August 31, 1953).

A2 F. A. Aschenbrenner, M.I.T. Laboratory for Nuclear Science, Progress Report (November 30, 1953).

A3 W. A. Aron, B. G. Hoffman, F. C. Williams, U.S.A.E.C. Bulletin No. AECU-663, republished by the Technical Information Service, Oak Ridge, Tennessee (May 28, 1951).

A4 F. Ajzenberg and T. Lauritsen, Revs. Modern Phys. 24, 321 (1952).

B1 S. T. Butler, Proc. Phys. Soc. (London) 208, 559 (1951).

B2 C. F. Black, Ph.D. Thesis, M.I.T., February 1953.

C1 E. T. Clarke and J. W. Irvine, Phys. Rev. 66, 231 (1944).

F1 W. Franzen and J. G. Likely, Phys. Rev. 87, 666 (1952).

G1 H. E. Gove, J. A. Harvey, M. S. Livingston, K. Boyer, and M. Zimmerman, M.I.T. Laboratory for Nuclear Science and Engineering, Progress Report (April 1, 1950).

G2 H. E. Gove, M. I. T. Laboratory for Nuclear Science and Engineering, Progress Report (July 1, 1950).

G3 E. Guth and C. J. Mullin, Phys. Rev. 82, 141 (1951).

H1 J. A. Harvey, Phys. Rev. 81, 353 (1951).

H2 J. A. Harvey, Ph.D. Thesis, M.I.T., May 1950.

J1 C. W. Johnstone, Los Alamos, private communication.

J2 C. W. Johnstone, Nucleonics, 11, 36 (1953).

L1 M. S. Livingston, J. Appl. Phys. 15, 2 (1944).

L2 M. S. Livingston and H. A. Bethe, Revs. Modern Phys. 1, 263 (1937).

O1 J. R. Oppenheimer and M. Phillips, Phys. Rev. 48, 500 (1935).

P1 D. C. Peaslee, Phys. Rev. 74, 1001 (1948).

S1 H. F. Stoddart and H. E. Gove, Phys. Rev. 87, 262 (1952).

T1 C. J. Taylor, W. K. Jentschke, M. E. Remley, F. S. Eby, and P. G. Kruger, Phys. Rev. 84, 1034 (1951).

T2 W. Tobocman, unpublished.

W1 N. S. Wall, Ph.D. Thesis, M.I.T., October 1953.

B I O G R A P H I C A L N O T E

Born:	June 26, 1924, Ellis, Kansas
Colleges Attended:	Kansas State College, 1947 - 1950 Massachusetts Institute of Technology, 1950 - 1954
Degrees Obtained:	B. S. with High Honors, 1950, Kansas State College
Professional Experience:	Teaching Fellow, M.I.T., 1950 - 1951 Technical Engineer, Summer 1951 General Electric Company Teaching Assistant, M.I.T., 1951 - 1952 Research Assistant, M.I.T., 1952 - 1954